AD-A050 757 PURDUE UNIV LAFAYETTE IND PROJECT SQUID HEADQUARTERS F/G 17/8
AN OPTICAL PARTICLE-SIZING COUNTER FOR IN-SITU MEASUREMENTS.(U)
JAN 78 D HOLVE, S A SELF N00014-75-C-1143
UNCLASSIFIED SQUID-SU-2-PU NL

| OF |
AD
A050757

END
DATE
FILMED
4-78
DDC

(12)

PROJECT SQUID
TECHNICAL REPORT SU-2-PU

see back page for 1473

AN OPTICAL PARTICLE-SIZING COUNTER FOR IN-SITU MEASUREMENTS

by

DON HOLVE AND SIDNEY A. SELF
MECHANICAL ENGINEERING DEPARTMENT
STANFORD UNIVERSITY
STANFORD, CALIFORNIA 94305

PROJECT SQUID HEADQUARTERS
CHAFFEE HALL
PURDUE UNIVERSITY
WEST LAFAYETTE, INDIANA 47907

JANUARY 1978

Project SQUID is a cooperative program of basic research relating to Jet Propulsion. It is sponsored by the Office of Naval Research and is administered by Purdue University through Contract N00014-75-C-1143, NR-098-038.

Technical Report SU-2-PU

PROJECT SQUID

A COOPERATIVE PROGRAM OF FUNDAMENTAL RESEARCH
AS RELATED TO JET PROPULSION
OFFICE OF NAVAL RESEARCH, DEPARTMENT OF THE NAVY

CONTRACT N00014-75-C-1143 NR-098-038

AN OPTICAL PARTICLE-SIZING COUNTER FOR IN-SITU MEASUREMENTS

BY

DON HOLVE AND SIDNEY A. SELF
HIGH TEMPERATURE GASDYNAMICS LABORATORY
MECHANICAL ENGINEERING DEPARTMENT
STANFORD UNIVERSITY
STANFORD, CALIFORNIA 94305

JANUARY 1978

PROJECT SQUID HEADQUARTERS
CHAFFEE HALL
PURDUE UNIVERSITY
WEST LAFAYETTE, INDIANA 47907

AN OPTICAL PARTICLE-SIZING COUNTER FOR IN-SITU MEASUREMENTS

By

Don Holve and Sidney A. Self

High Temperature Gasdynamics Laboratory
Mechanical Engineering Department
Stanford University
Stanford, California

ABSTRACT

A particle sizing counter is described, suitable for in-situ measurements in two phase flows of laboratory scale. It employs near-forward scatter from the focus of a He-Ne laser beam, together with pulse height-analysis of the signals from individual particles. A novel and essential feature of the technique is a numerical inversion scheme to unfold the dependence of the scattered signals on particle trajectory through the measurement volume. The inversion procedure is performed by an on-line computer, and utilizes a prior calibration with monodisperse aerosols of known size. As presently configured, the instrument has a demonstrated capability of determining size distributions in the diameter range 2-25 μm, at concentrations up to $\sim 10^5$ cm^{-3}. The measured dependence of response on particle diameter agrees well with calculations from Mie scattering theory. It is anticipated that the technique can be extended to cover particle diameters up to at least 50 μm, and down to 0.5 μm and concentrations up to 10^6 cm^{-3}. It should also be adaptable to hot flows and absorbing, irregular particles.

Table of Contents

List of Tables

List of Figures

1.0 INTRODUCTION

The measurement of particle size distributions in two phase flows is of considerable current interest, especially in connection with energy conversion devices such as liquid spray and pulverized fuel combustors, and particulate cleanup devices such as electrostatic precipitators. While the particulate characteristics, such as mean diameter, size distribution, mass loading etc., may vary quite widely in such systems, the sizes of interest generally fall in the range 0.5 - 50 μm, with concentrations up to 10^6 cm^{-3} (for the smaller sizes).

The available measurement techniques [1,2] also vary widely in type and capability. Several, including microscopy, cascade impactors, Coulter counters, mobility analyzers and commercial optical counters require a sample to be extracted from the flow. This poses problems related to obtaining a representative sample, especially for the larger sizes and in hot, high velocity flows. Also, many sampling methods are cumbersome and slow in operation. For these reasons optical techniques are of especial interest since, in principle, they are capable of making in situ measurements with continuous and rapid readout. Moreover, by using lasers, they are adaptable to high temperature systems having high thermal radiation background.

Optical techniques all depend on Mie scattering [3,4], and can be broadly divided into imaging and non-imaging types. The former, including flash photography [5] and holography [6], are limited in practice to sizes $\gtrsim$ 30 μm, and pose a difficult data reduction problem. Non-imaging methods can be subdivided into two classes: those which measure on a large number of particles simultaneously, and those which count and size individual particles, one at a time.

The former type includes the well-established transmissometer [7,8], which measures the extinction of a light beam and yields a value for the integrated projected area of the particles in the beam. It does not allow point measurements, and requires another measure, such as the mass loading, to yield a mean diameter. Other techniques have been described [9-11] which measure the angular distribution of light scattered from a large number of particles simultaneously present in a small measurement volume. They yield either some moments of the distribution [9,10] or require the angular distribution to be unfolded to give the size distribution [11].

Sampling-type optical counter-sizers for gas flows have been commercially available for some years. The sample is diluted as necessary, and constrained to flow through a small jet (~ 1 mm dia.) which is uniformly illuminated with a collimated white light beam. The scattered light pulses are collected, usually in forward scatter, detected and pulse-height analyzed to give a number-size distribution. Apart from a limitation to particles $\lesssim$ 10 μm and the need for sampling and sample dilution, the main problem with such counters [12,13] is the achievement of a response which is insensitive to particle refractive index.

A novel interferometric approach to in-situ particle counting-sizing has been suggested by Farmer [14,15] and by Durst [16], making use of the shape of the signals scattered by single particles passing through the fringes in the cross-over volume of a dual beam laser anemometer. A simple analysis [14] suggests that the signal visibility is a monotonic function of the ratio particle diameter/fringe spacing, in a certain range, and is independent of scattering angle and refractive index. However, more detailed analyses [17] from Mie theory and experiments [18] indicate a complicated dependence on these parameters, which raises questions concerning the method's utility except, perhaps, in a suitably engineered forward scatter geometry.

Apart from this interferometric method, there appear to be two basic types of approach to devising an in situ particle sizing counter. In the first, the absolute scattered signal amplitude in a single collection-detection channel is employed, as in commercial, sampling type optical counters. In the second, use is made of the relative amplitudes of the scattered signals in two or more detector channels set at different angles [19].

In this paper we describe the development of an in-situ, forward scatter laser particle sizing counter following the former approach. It has a demonstrated capability on cold, small scale, low velocity flows of sizing particles in the range 2 - 25 μm at concentrations up to at least 10^5 cm^{-3}. In its present form the instrument will accommodate flows up to 40 cm in width. By adjusting the instrumental parameters to suit the particle characteristics, it should be possible to extend the range downwards to ~ 0.5 μm and upwards to $\gtrsim$ 50 μm, and handle concentrations to 10^6 cm^{-3}. Moreover, estimates indicate that the instrument should be applicable to hot, radiant flows, at least on laboratory scale systems.

There are two major factors involved in the practical realization of an instrument of this type. The first concerns the control of the size and shape of the effective measurement volume, and the uniformity of response for different particle trajectories through it; this is discussed in Section 2. The second relates to the attainment of a response which is, as near as possible, monotonic with particle size, and which has minimal sensitivity to particle refractive index; this is treated in Section 3. As discussed later, these two factors are coupled in such a way that the optimum trade-off is a function of the size range and concentration to be measured.

From the discussion of Section 2 it transpires that the response for different trajectories is quite non-uniform. Hence, as experimental tests show, a flow of monodisperse particles yields a signal amplitude-count distribution with a sharp cut-off at some maximum signal value, and a spread to lower values. It has been found possible, however, to use a numerical inversion scheme, based on experimental calibrations with monodisperse particles, to unfold this distribution of signal amplitudes to obtain the true size. This technique, which is a vital feature of the present scheme is developed in Section 4.

Section 5 details the results of calibration tests on monodispersions and polydispersions. The latter demonstrate the instrument's ability to correctly resolve the structure in the distribution.

The paper is concluded with a discussion of the extension of the technique to a wider size range and its application to hot flow systems.

2.0 MEASUREMENT VOLUME CONSIDERATIONS

The characteristics of the measurement volume are a crucial factor in the design of an in-situ optical sizing counter because the particle trajectories are not controlled as they are in a sampling-type optical counter.

The effective measurement volume is determined in part by the intensity distribution in the illuminating beam, and in part by the geometry of the collection optics, including stops and apertures. Ideally, the measurement volume should be of roughly spherical or cubical shape with a uniform illumination intensity, and a uniform light collection efficiency for points within the volume. Otherwise, the peak scattered intensity will depend on trajectory, so that signals from large particles traversing the edge of the volume may be comparable with those from small particles traversing the center.

The linear dimensions of the measurement volume should be several (2 or 3) times larger than that of the largest particles to be measured, so that the fraction of such particles which follow edge trajectories yielding sub-standard signals is small. For a measurement volume satisfying this criterion, there will clearly be a limit of useful operation set by the occurrence of a significant fraction of coincidences when two particles are simultaneously present in the volume, giving rise to erroneous signals. This condition, which sets a limit to the maximum measurable concentration of the more numerous small particles, is analyzed in Appendix I. It should be emphasized that the capability of handling concentrations up to the range of $10^5 - 10^6$ cm^{-3} is necessary for many flow systems of interest. Roughly, it can be said that for an effective measurement volume of $V_m cm^3$, the maximum concentration that can be measured without significant interference due to coincidence is $N_{max} \sim V_m^{-1}$ cm^{-3}.

Concerning the distribution of intensity in the illuminating beam, assuming a TEM_{oo} laser, the profile is Gaussian, and by suitable optics can be focused to a waist at the measurement station. Using cylindrical coordinates centered at the waist, the intensity distribution is

$$I(r,z) = \frac{2P}{\pi w^2} \exp\left[-2(r/w)^2\right] \qquad (2.1)$$

where P is the beam power and the beam radius (to $1/e^2$ intensity) is

$$w(z) = w_o [1 + (\lambda z/\pi w_o^2)^2]^{1/2} \tag{2.2}$$

Here w_o is the beam radius at the waist ($z = 0$) and is given in terms of the far field half angle of convergence, θ_b, by

$$w_o = \frac{\lambda}{\pi \theta_b} \tag{2.3}$$

Thus a Gaussian intensity profile (which is a reasonably good approximation to the ideal rectangular profile) with a waist diameter in the range of interest (~ 100 μm) can be readily created by suitable beam expansion and focusing, and involves conveniently small beam convergence/divergence angles.

It may be noted that by using cylindrical rather than spherical lenses, ribbon beams with Gaussian profiles having distinct waist widths in orthogonal directions (x,y) can also be created, and offer certain advantages.

The intensity distribution along the beam (z) axis is Lorentzian and falls off much more slowly than with radius. The Rayleigh distance z_R, where the intensity on axis falls to half the central waist intensity, is

$$z_R = \pi w_o^2/\lambda \tag{2.4}$$

For waist diameters of interest ($2 w_o$ ~ 100 μm) and visible lasers, z_R ~ 1 cm, so that the illumination volume is typically very long compared with its width. Clearly, then, it is necessary to limit the effective length of the measurement volume in the z direction by suitable design of the collection optics.

The most direct method of achieving this is to use a lens on a collection axis at some angle θ_c to the forward direction of the laser beam, and image the laser waist onto a pinhole aperture, as shown in Figure 1. Clearly, from the point of view of limiting the length of the measurement volume, a choice of θ_c ~ 90° is most effective. On the other hand, as discussed in Section 3 below, to satisfy the requirements of a monotonic signal/size response, with least sensitivity to refractive index, a coaxial forward scatter geometry ($\theta_c = 0$) is most desirable; moreover the satisfaction of these requirements becomes more difficult as the scattering angle θ_c is increased.

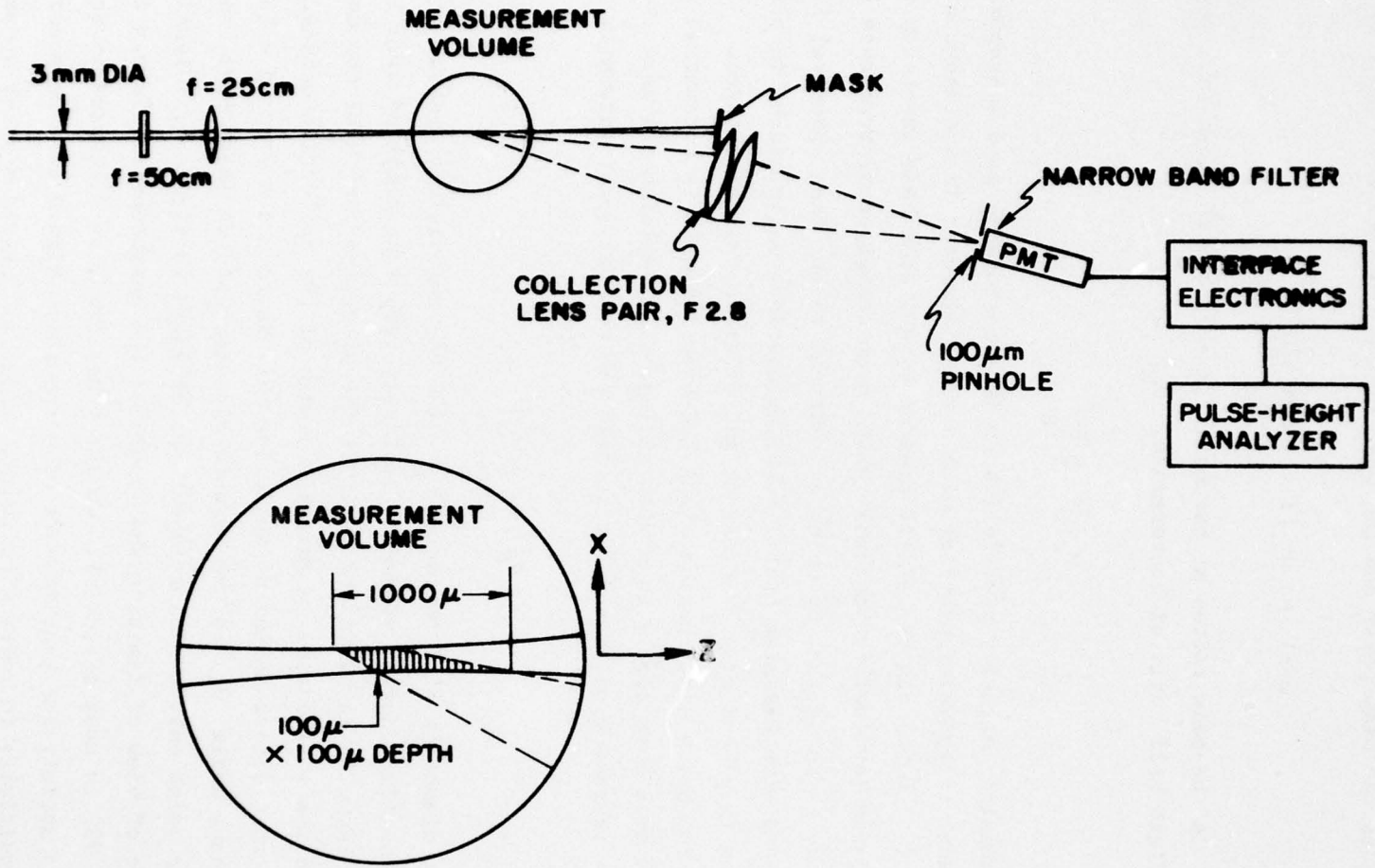

Figure 1. Schematic of Optical System

In an attempt to retain a coaxial forward scatter geometry, and to delimit the length of the measurement volume, the use of a central stop on the collection lens was investigated. However, a practical solution did not appear possible with this configuration. Consequently it was found necessary to effect a compromise between the conflicting requirements of limiting the length of the control volume and achieving a satisfactory response, by using an off-axis, near-forward scatter geometry with θ_c in the range 10 - 20°, as shown in Figure 1.

In the particular system investigated the illumination is provided by a 2 mW He-Ne TEM_{oo} mode laser, which is focused by cylindrical lenses to a ribbon beam with waist widths (to $1/e^2$ intensity) of approximately $2\ w_x \sim$ 100 μm x $2\ w_y \sim$ 300 μm, with a waist length greater than 1 cm. The collection axis is in the x-z plane at an angle θ_c to the z-axis. The collection lens, consisting of a back-to-back pair of good quality f/2·8, 25 cm focal length lenses, designed for infinite conjugate ratio, images the center of the beam waist to the center of a pinhole aperture of diameter $2\ w_A \sim 100$ μm diameter, with unity magnification. Thus the viewed volume is approximately a cylinder of diameter 100 μm intersecting the ribbon beam at an angle θ_c, while the measurement volume is given approximately by the intersection of the viewed volume and the illuminating beam. From geometrical considerations the measurement volume can be characterized roughly as a cylinder with slant ends, of diameter $2\ w_A \sim 100$ μm, length $2\ w_x/\sin\theta_c \sim 1000$ μm for angles of interest, and volume $V_m \sim 10^{-5}$ cm^{-3}. The particle flow is directed in the y-direction.

The foregoing arguments defining the measurement volume are, of course, only approximate. A rigorous treatment should consider the angular distribution of intensity scattered from a particle of given size at a given position in the illuminating beam, and thence a calculation made of the intensity distribution in the plane of the pinhole produced by the light intercepted by the collection lens, to obtain the detected signal as a function of particle size and position. Fortunately, such an involved calculation is circumvented by the calibration procedures described in Section 5..

In any event, it is clear that the use of forward scatter at small angles results in a distribution of intensity in the measurement volume which is quite non-uniform, although the use of a ribbon laser beam reduces the non-

uniformity in the y direction. Consequently the scattered signal is trajectory dependent, and a flow of monodisperse particles yields a signal peak amplitude count distribution having a sharp cut off at some maximum signal value, corresponding to particles traversing the center of the measurement volume, with a spread to smaller amplitudes.

To overcome this problem of nonuniformity of response within the measurement volume, a numerical inversion scheme, combined with a calibration procedure has been devised, as discussed in Section 4, to unfold the distribution of signal amplitudes and yield an indicated size distribution which eliminates the dependence on trajectory.

3.0 OPTIMAL COLLECTION GEOMETRY; SCATTERING THEORY

Highly desirable, if not essential, requirements for an effective optical sizing counter is a monotonically increasing dependence of signal amplitude on particle size, and insensitivity to the complex refractive index $\tilde{n} = n_1 + in_2$ of the particle (where the imaginary part represents absorption).

To find an optimal geometry for satisfying these requirements entails extensive parametric calculations of the response for different geometries as a function of particle size and refractive index from Mie scattering theory. The latter gives the differential scattering amplitude for a spherical particle in an incident monochromatic plane-polarized wave, as a function of scattering angle θ, polarization, complex refractive index $\tilde{n}$, of the particle (relative to the medium) and the normalized size parameter $\alpha \equiv \pi d/\lambda$, where d is the diameter and λ the wavelength. This scattering amplitude must then be integrated over the aperture of the collection optics to give the response.

Unfortunately the Mie scattering function is an extremely complicated and sensitive function of the parameters θ, α, $\tilde{n}$, which is difficult to characterize in simple terms, although fast computer codes are now available for its evaluation. However, as discussed by Hodkinson [20], in the limit of large particles, $\alpha \gtrsim 3/(n_1 - 1)$, i.e. $d \gtrsim 2\lambda \sim 1$ μm, a very good insight can be obtained by considering the separate effects of diffraction, refraction and reflection. Fifty per cent of the total scattered power is attributable to diffraction and is distributed in the well known and easily characterized Fraunhoffer diffraction pattern of a circular disk or aperture, which is the same as that of a spherical particle and is independent of polarization and of the refractive index.

For such diffraction, the differential scattering efficiency, defined as the flux scattered per unit solid angle divided by the flux incident on the particle projected area, is

$$I_{diff} = \frac{\alpha^2}{4\pi}\left[\frac{2\,J_1(\alpha \sin\theta)}{\alpha \sin\theta}\right]^2 , \qquad (3.1)$$

where J_1 is the Bessel function of the first kind and order one. This function represents the familiar central lobe surrounded by bright rings of decreasing intensity. The first zero or dark ring occurs at

$\alpha \sin \theta = 3.83$. For $\alpha \gtrsim 6$, and $\lambda = 0.633$ μm, the first zero occurs for $\theta_1 \sim 44°/d(\mu m)$.

The integrated scattering efficiency is given by

$$I_{int} = 2\pi \int_o^{\theta} I_{diff} \sin \theta \, d\theta = 1 - J_o^2 (\alpha \sin \theta) - J_1^2 (\alpha \sin \theta). \quad (3.2)$$

Approximately 85% of the diffracted flux falls in the central lobe.

This result leads to the following attractive concept for particle sizing; if the flux is collected coaxially by a lens, the signal will be monotonic with size and independent of refractive index. Moreover, for a lens aperture of θ_{max}, the signal will be closely proportional to d^2 for $d(\mu m) \gtrsim 44°/\theta^o_{max}$. For instance, for $\theta_{max} \sim 10°$ corresponding to F/2.8 collection aperture, this will hold for $d \gtrsim 4$ μm. Of course there is also an upper limit to the size which yields a signal $\propto d^2$, in view of the need to stop off the center of the lens to block the unscattered beam.

As mentioned in Section 2, the use of such a coaxial forward scatter geometry was investigated, but it was abandoned in view of the difficulty of limiting the axial length of the measurement volume for reasonable collection apertures. Consequently, to obtain a measurement volume small enough to handle concentrations of practical interest, one is forced to accept an off-axis scattering geometry.

This requires computations from the full Mie theory, but the foregoing analytic results from diffraction theory with coaxial collection lead one to expect that, provided one keeps the central scattering angle θ_c small, then the response will not depart far from monotonicity and the dependence on refractive index will be weak. One also anticipates that, in general, the use of a wide collection aperture and the use of white light will also favor the attainment of the desired requirements, since both will tend to average over the detailed resonant structure characteristic of Mie scattering.

Lieberman and Allen [21] have reported experimental and theoretical results for the response of a coaxial, near forward scatter configuration. corresponding to a commercial sampling-type optical counter employing white light. Scattered light is collected coaxially between angles of 15.5° and 28°. The relative response as a function of particle diameter for latex

($\tilde{n} = 1.6 + i.0$) and glass spheres is reproduced in Figure 2. The curve shows a generally increasing dependence on d, approximately proportional to d^2, over the range $d = 0.3$ μm to 50 μm, with the exception of a dip or resonance in the neighborhood of 1 μm. Specifically, the response is double valued for the interval $d = 0.65$ μm to 1.2 μm, and such behavior is characteristic of instruments of this type. In practice, signals from particles in this size range are lumped into a single size bin in the pulse height analyzer. For many purposes this is perfectly adequate, such a 2:1 size resolution increment being comparable with that achieved by cascade impactors over the whole size range.

A systematic calculation of the response curve for a coaxial forward scatter system, as a function of the collection aperture between scattering angles θ_1 and θ_2 ($> \theta_1$) was made by Oeseburg [22] for spherical particles of $\tilde{n} = 1.49 + i.0$, and for size parameter up to $\alpha = 30$ (corresponding to $d \sim 6$ μm for $\lambda = 0.63$ μm). It was found that a resonant dip around $\alpha \sim 5$ ($d \sim 1$ μm) was a persistent feature over wide ranges of the aperture angles θ_1 and θ_2, and that, for many apertures, additional resonances occurred at several larger α values. A measure of the magnitude of a resonant dip can be defined by $R = 2\,(\alpha_L - \alpha_S)/(\alpha_L + \alpha_S)$, where α_S and α_L represent the smaller and larger size parameters, respectively, which give double-valued responses. Thus R represents the size resolution increment for which signal amplitudes must be lumped into one size bin, and has a value ~ 0.6 for the case discussed above.

Oeseburg found that only by going to values of $\theta_1 > 20°$ combined with very large values of $\theta_2 \sim 120°$, could the R value for all dips be significantly reduced. The optimum aperture for the chosen refractive index occurred for $\theta_1 = 40°$, $\theta_2 = 120°$, and yielded a response with no dips having R values greater than 0.15.

It should be emphasized that while such very large apertures are feasible in sampling-type optical counters through the use of ellipsoidal mirror collectors surrounding the measurement volume, they are quite infeasible for in-situ instruments. For a useful instrumental throw between the measurement point and the collecting optics, large apertures entail expensive, large diameter lenses. For example, the collecting lenses used in the present work,

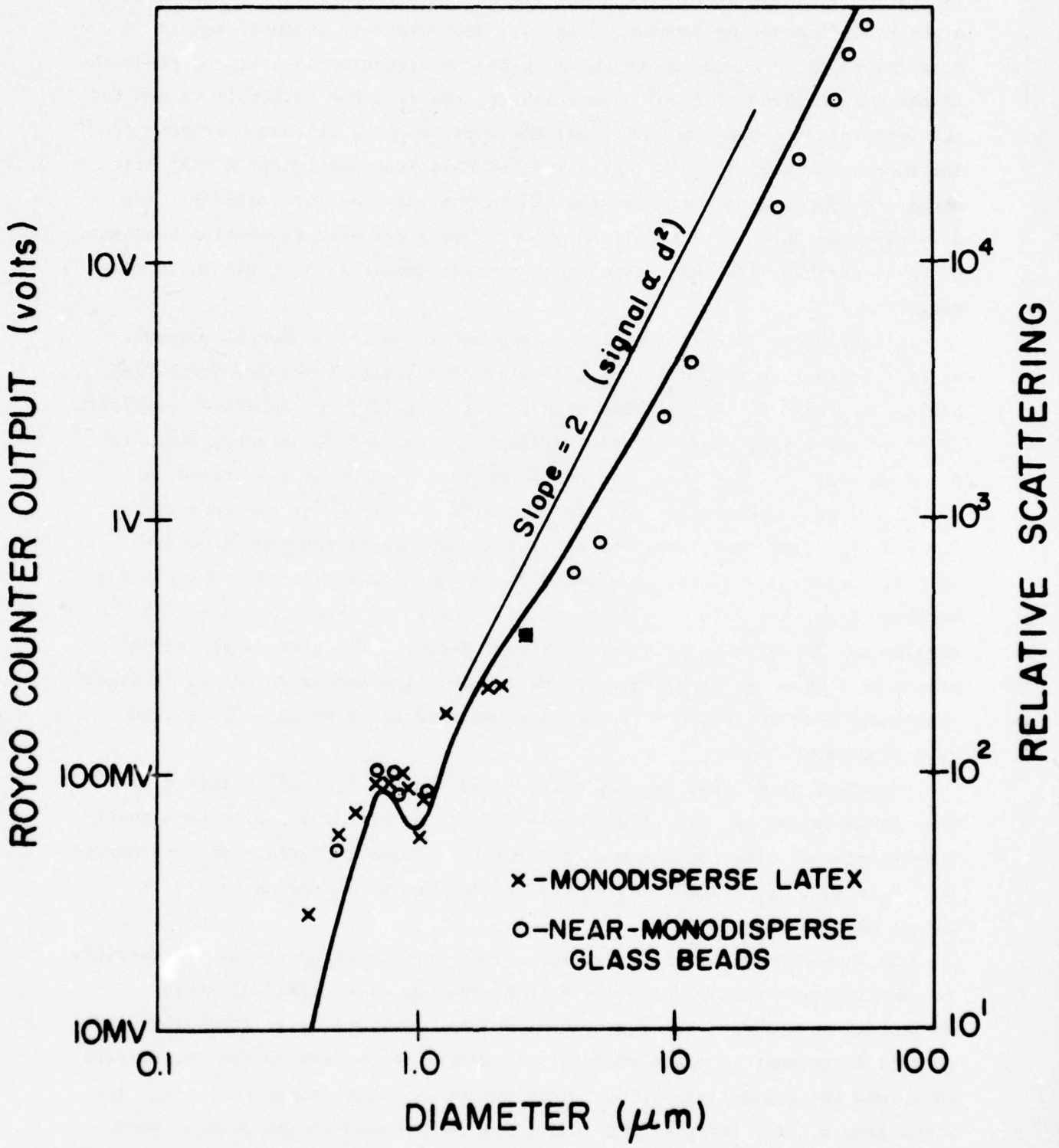

Figure 2. Response Function for a Royco Counter Using White Light Illumination

of focal length 25 cm and diameter 9 cm (F/2.8) allow a maximum difference $(\theta_2 - \theta_1) \sim 20°$ when used for off-axis collection.

With these practical restrictions in mind, and guided by the general trends of the results of references 21, 22 and other similar published work, response calculations have been carried out for the collection geometry illustrated in Figure 3. The collection lens of aperture half angle $\theta_L = \tan^{-1}(1/2F)$ is centered on the collection axis at an angle of θ_c. Allowance is made for the presence of a planar mask which blocks light scattered out to an angle $\theta_m \geq (\theta_c - \theta_L)$, and the response is calculated by integrating the intensity over the remaining portion of the lens, shown unshaded in Figure 3.

The calculation of the response function proceeds as follows. For spherical particles, van de Hulst [3] gives the basic relation

$$\underset{\sim}{I} = \frac{1}{k^2 r^2} \underset{\sim}{F'}(\alpha,\theta,n) \cdot I_o \tag{3.3}$$

where I_o (power/unit area) is the intensity of the incident plane wave, I is the intensity of the scattered spherical wave at radius r from the particle, $k \equiv 2\pi/\lambda$ is the wavenumber, and F' is the dimensionless scattering matrix.

The intensities are four-vectors in terms of the Stoke's parameters

$$\underset{\sim}{I} \equiv \begin{vmatrix} I_e \\ I_r \\ u \\ v \end{vmatrix} \tag{3.4}$$

and

$$\underset{\sim}{F'} \equiv \begin{vmatrix} M_2 & 0 & 0 & 0 \\ 0 & M_1 & 0 & 0 \\ 0 & 0 & S_{21} & D_{21} \\ 0 & 0 & D_{21} & S_{21} \end{vmatrix} \tag{3.5}$$

For an unpolarized incident beam, Eqn. (3.3) reduces to

$$I = \frac{1}{k^2 r^2} \left(\frac{M_1 + M_2}{2} \right) I_o \tag{3.6}$$

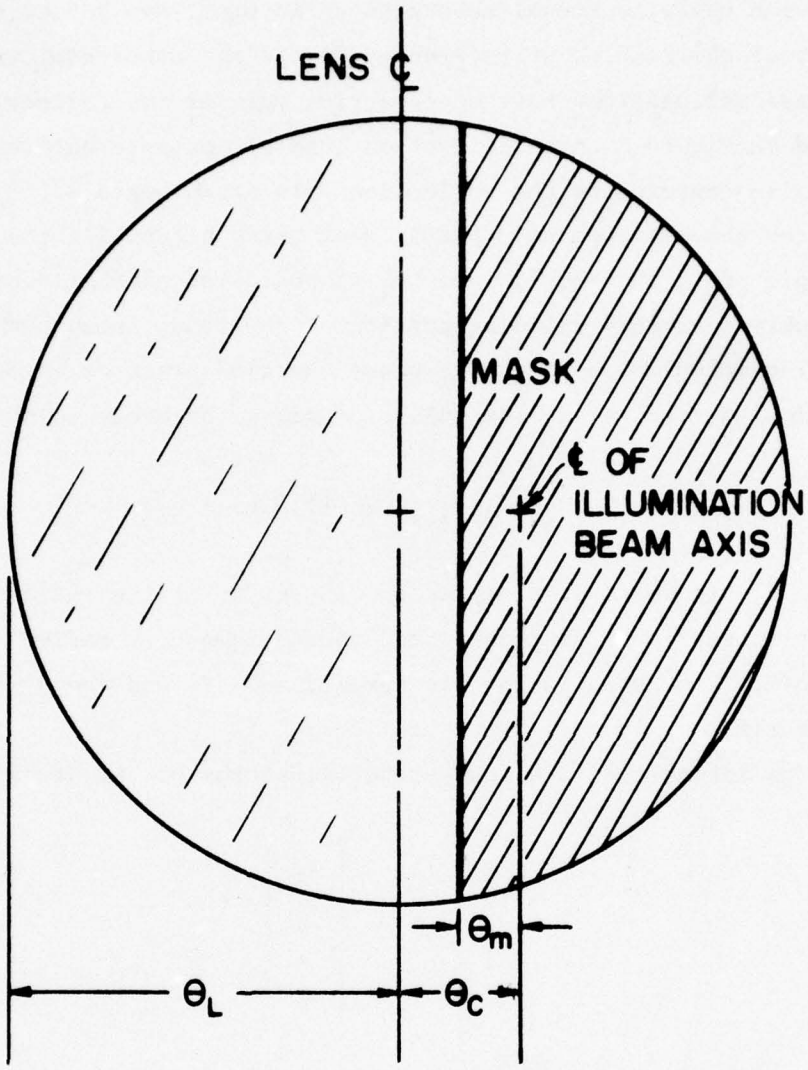

Figure 3. Scattered Light Collection Geometry
for Present Optical System

The scattered power collected in an aperture of area $A = r^2\Omega$, where Ω is the solid angle for collection is given by

$$P = \frac{I_o \lambda^2}{4\pi^2} \int_\Omega \left(\frac{M_1 + M_2}{2} \right) d\Omega \tag{3.7}$$

$$= \frac{I_o \lambda^2}{4\pi^2} F(\alpha, \tilde{n}, \Omega) \tag{3.8}$$

where the dimensionless response function is defined by

$$F(\alpha, n, \Omega) = \int_\Omega \left(\frac{M_1 + M_2}{2} \right) d\Omega \tag{3.9}$$

and is the effective scattering cross-section for the particular collection geometry, normalized by λ^2.

The matrix elements $M_1(\alpha, \theta, \tilde{n})$, $M_2(\alpha, \theta, \tilde{n})$ are computed by a code developed by Davé [23]. The response function F is then calculated by integrating $(M_1 + M_2)/2$ over the collection solid angle.

We have performed calculations on 65 sets of parameters, and although not exhaustive, the results from these calculations indicate general trends. The following figures (Figures 4-7) are representative and are chosen to illustrate the typical dependence of the response on the important parameters. To reduce the number of parameters all the curves shown are for the case $\theta_m = \theta_c$ i.e. with the inner half of the lens masked, although this may not make optimal use of the lens aperture. Also, an unpolarized beam was assumed, though the choice of a single polarization might well lead to an improved response.

Figures 4(a)-(c) show the response for $\tilde{n} = 1.6 + 0.0i$ and fixed minimum scattering angle $\theta_m = \theta_c = 4°$, for increasing values of the maximum scattering angle $(\theta_c + \theta_L)$ i.e. increasing aperture. Figures 5(a)-(d) show the response for the same refractive index and fixed aperture ($\theta_L = 20°$), for increasing values of scattering angle θ_c.

All of these curves exhibit a more or less pronounced resonance (dip) at $\alpha \sim 5$, together with a series of resonances of decreasing magnitude at larger α. This form is insensitive to the real part of the refractive index, n_1, especially at the small scattering angles, but the exact positions and shapes of the resonances do depend on n_1. In general the α values of the resonances scale as $(n_1 - 1)^{-1}$. The effect of increasing the aperture to include larger scattering angles (Figure 4) is to reduce the magnitude of the higher resonances but its effect on the first resonance at $\alpha \sim 5$ is slight.

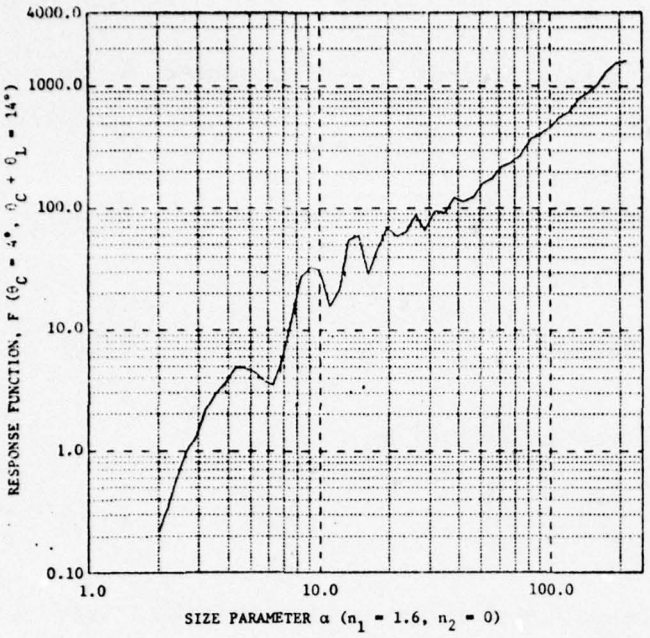

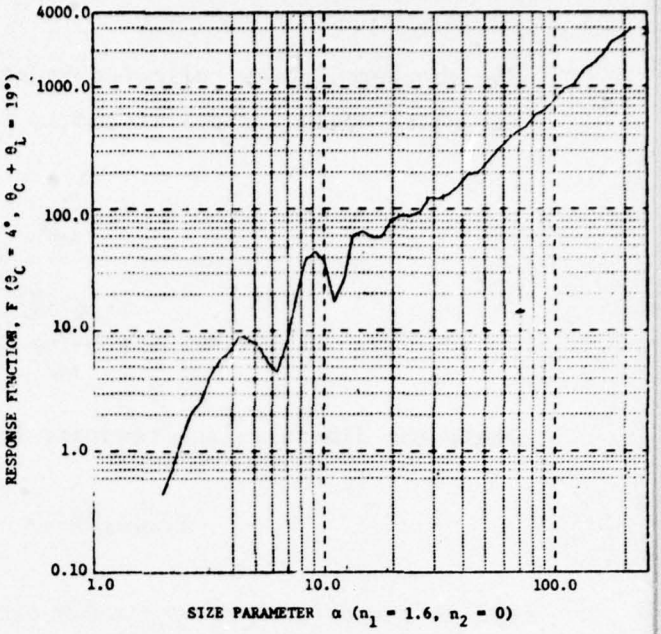

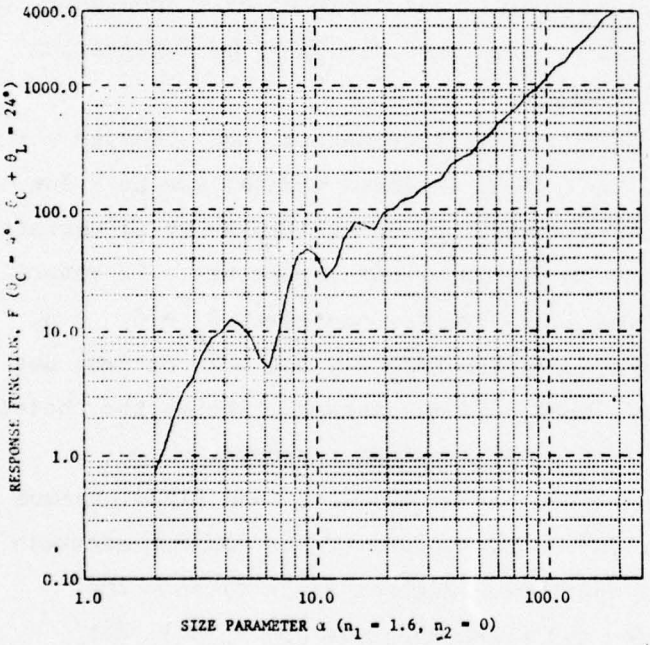

Figure 4. Variation of Response Function with θ_L for $\theta_c = 4^o$, $n_1 = 1.6$, $n_2 = 0.0$

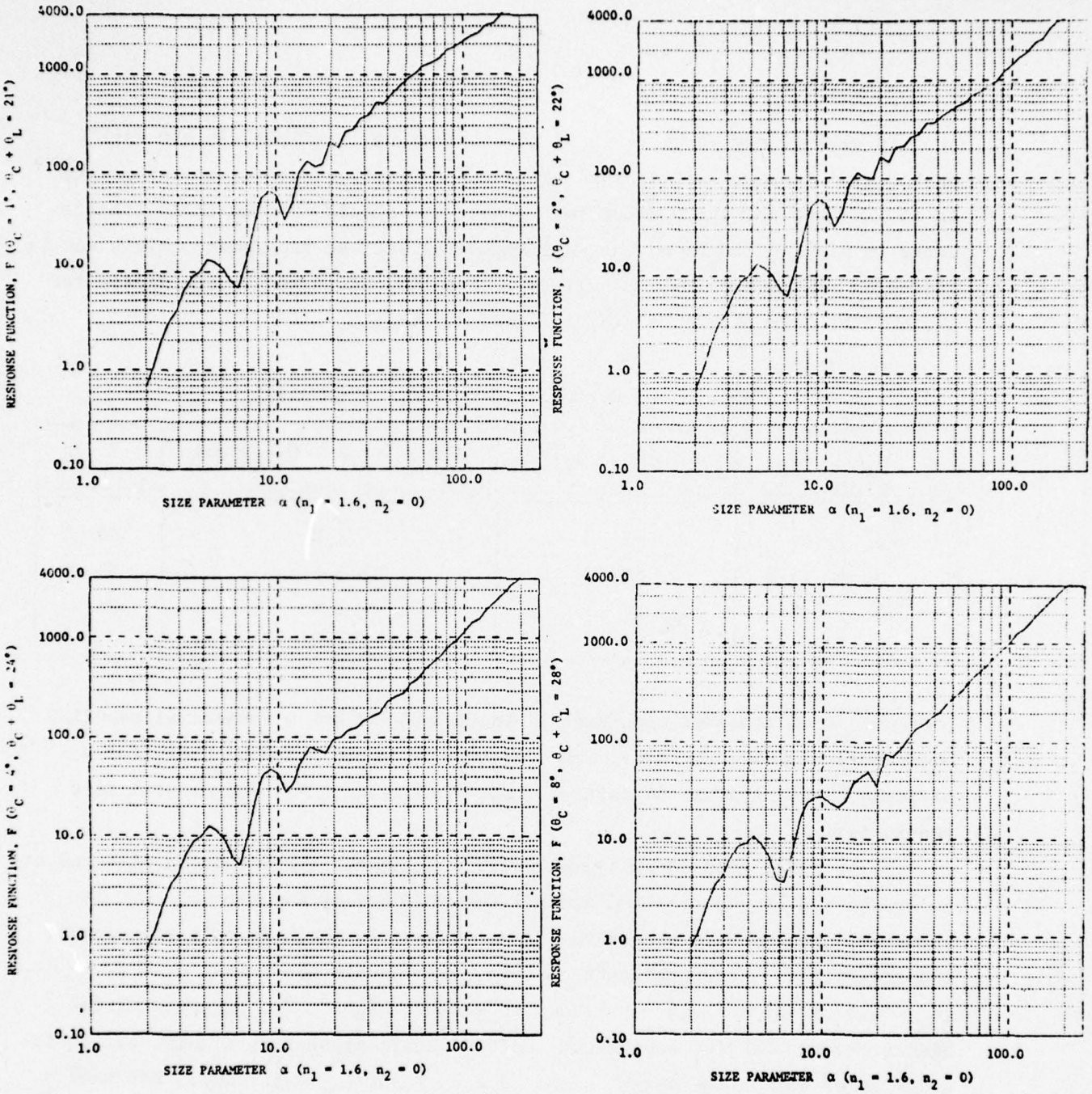

Figure 5. Variation of Response Function with θ_c for $\theta_L = 20^o$, $n_1 = 1.6$, $n_2 = 0.0$

In view of the persistence of the resonances, particularly the first, over a wide range of scattering angles and collection apertures appropriate to an in-situ, forward scatter instrument, one should examine their significance in placing limits on the performance of such an instrument. This can be discussed in terms of the R values of the resonances, which are listed for the typical case of Figure 4(b) in Table 3.1 below.

Table 3.1. Resonance Widths for Figure 4b.

α_S	α_L	$\bar{\alpha} = (\alpha_S + \alpha_L)/2$	$\bar{d}$(μm)(for λ = 0.633 μm)	R
3	7	5	1.0	.80
8	13.5	10.8	2.2	.51
15	19	17	3.5	.24

They should be compared with the R value of 0.60 for a commercial sampling counter as discussed by Lieberman [21], and with the value of 0.67 (for all particle sizes) typical of cascade impactors having a 2:1 incremental size resolution.

It is clear that an instrument with an acceptable performance with respect to resolution can be realized despite the presence of the resonances. The greatest limitation is set by the first resonance, which is only relevant if one attempts to design an instrument to work through the value $\bar{\alpha}_1 \sim 5$ ($\bar{d}_1 \sim 1.2$ μm for λ = 0.633 μm) down to smaller sizes. The presence of the higher resonances with smaller R values should present no significant limitation to measuring the larger sizes ($d \gtrsim 2$ m for λ = 0.633 μm). For many purposes, where high resolution in the range 1 μm is not required, a useful performance may well be obtained even through the region of the first resonance. Alternatively, the size range in question might be reduced by a factor ~ 2 by the use of a shorter wavelength e.g. from a He-Cd laser, which would also have the advantage of minimizing interference from thermal background in hot flows.

As noted above, for the range of scattering angles and collection apertures of interest, the dependence of the response on the real part of the refractive index over the limited range of practical interest ($n_1 \sim 1.3 - 1.7$ say) is

weak. However, for some important applications e.g. in coal combustion, there can be an appreciable imaginary component n_2 (i.e. absorption). For instance a value of $n_2 \sim 0.1$ corresponds to a highly absorbing material such as black coal, while values of $n_2 = 0.002 - 0.006$ corresponds to measured values [24] for the silicaceous slag in a coal-fired MHD channel.

Figures 6(a)-(d) show the response for a fixed collection geometry $\theta_m = \theta_c = 4°$, $\theta_L = 20°$ and $n_1 = 1.6$, for increasing values of n_2. The difference between $n_2 = 0$ and $n_2 = 10^{-3}$ is negligible, but for $n_2 = 10^{-2}$, the slope of the smooth, large α ($\alpha \gtrsim 20$) part of the response is significantly reduced, leaving the lower α part, including the resonances, virtually unchanged. Further increase of n_2 to 10^{-1} produces a smoothing of the resonances to yield a monotonic response. Figures 7(a)-(d) parallel those of Figures 6 except that a smaller minimum scattering angle $\theta_m = \theta_c = 1°$ is used. The main difference is that the sensitivity to n_2 of the slope at large α is reduced. Thus for large particles, a small scattering angle should be used to minimize sensitivity to absorption.

In concluding this section, certain general statements can be made as follows. For practical ranges of scattering angle and aperture appropriate to an in situ instrument, an adequately monotonic response function can be achieved to allow useful resolution over the size range $\alpha \gtrsim 5$, and possibly to smaller sizes, and with a relatively weak sensitivity to complex refractive index $\tilde{n}$. However, for accurate results it would be desirable to calibrate the instrument using monodispersions of particles with the refractive index of interest. In general, for the larger sizes, small scattering angles should be used to minimize sensitivity to $\tilde{n}$, while for the smaller sizes, larger scattering angles should be used to minimize the measurement volume and hence raise the maximum concentration that can be handled.

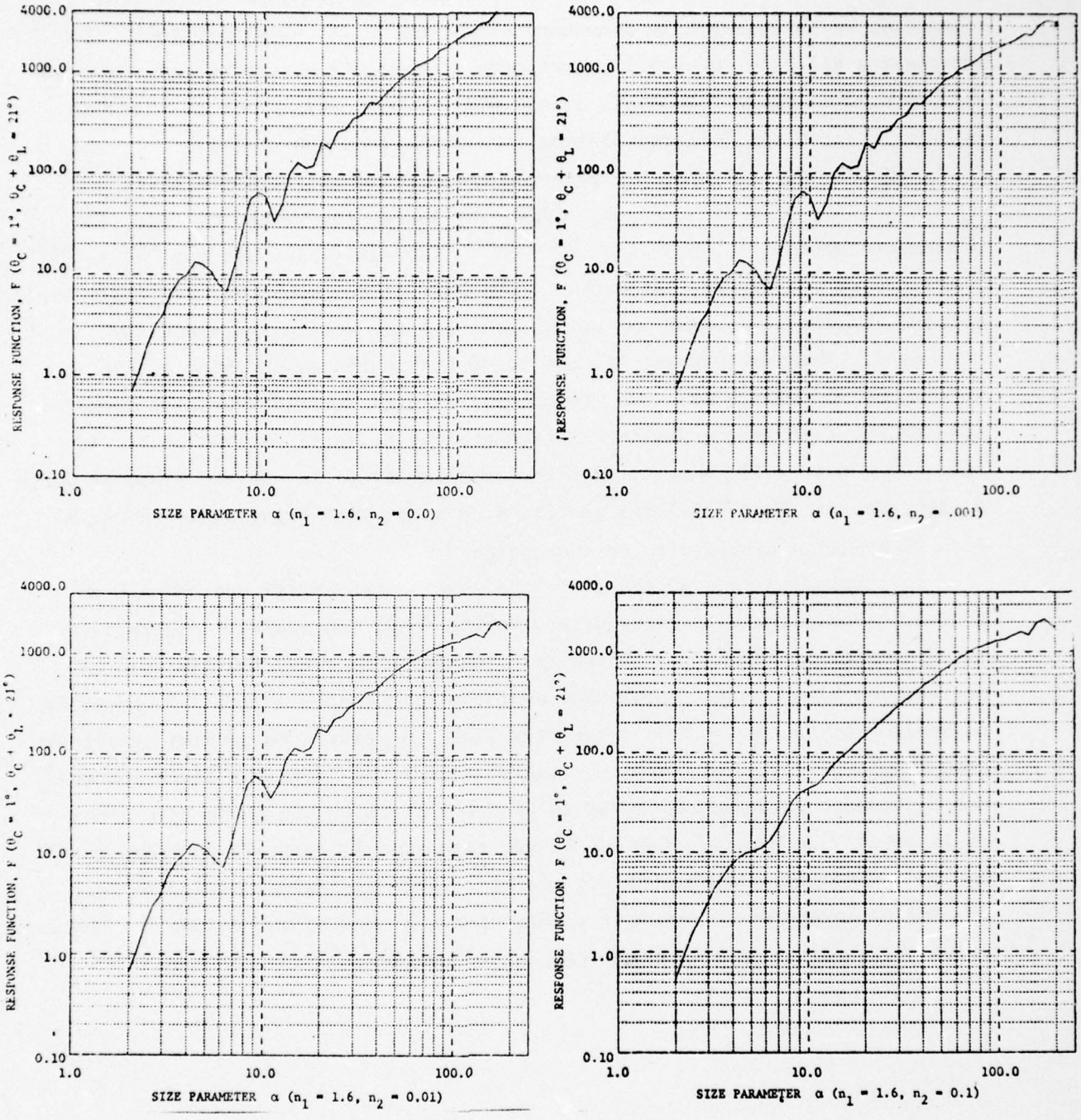

Figure 6. Variation of Response Function with Complex Refractive Index n_2 (Absorption) for $\theta_c = 1^o$, $\theta_L = 20^o$, n_1 - 1.6

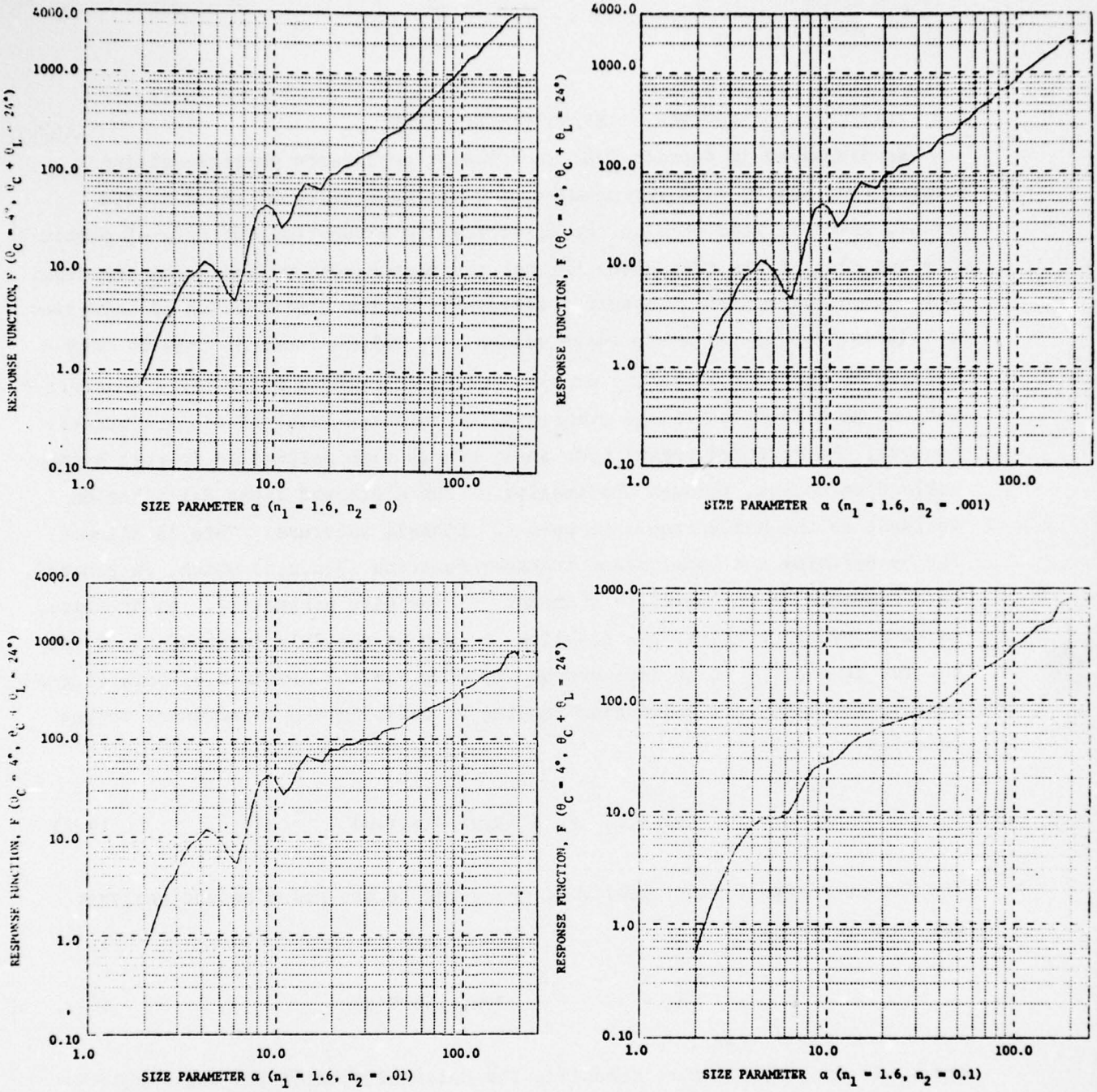

Figure 7. Variation of Response Function with Complex Refractive Index n_2 (Absorption) for $\theta_c = 1^o$, $\theta_L = 20^o$, $n_1 = 1.6$

4.0 TRAJECTORY DEPENDENCE - INVERSION TECHNIQUE

As discussed in Section 2.0, in devising an in-situ particle-sizing counter, one has to face the problem that the peak value of the detected signal, which is used to size the particles, is a function not only of particle size but also of its trajectory through the measurement volume. The principal factor controlling this trajectory dependence is the distribution of intensity of illumination in the measurement volume. To take account of this we define $I_o(x,z)$ as the peak intensity experienced by a particle following a y-directed motion, as a function of the transverse coordinates (x,z) of its trajectory. However, the detected signal peak amplitude is also determined in part by the collection optics, through the imaging of the scattered light distribution incident on the collection lens onto the pinhole aperture. This is allowed for by defining a dimensionless transfer function $H(x,z,\alpha)$ which, in general, is a function of the particle diameter d (or size parameter). In practice, as measurements confirm, the function H can be sensibly independent of d, but for generality it is included by allowing for the combined effects of non-uniform intensity and collection/imaging by defining the measurement volume function

$$J(x,z,\alpha) = I_o(x,y)\, H(x,z,\alpha) \tag{4.1}$$

The detected signal peak amplitude, delivered to the pulse height analyzer can then be written

$$A = G \cdot \frac{\lambda^2}{4\pi^2} J(x,z,\alpha)\, F(\alpha) \tag{4.2}$$

where G is a constant representing the detector sensitivity and electronic gain, and $F(\alpha)$ is the response function defined in Section 3.0 for particles of size parameter α illuminated by a uniform plane wave. It may be noted that, especially for particles large compared with the linear dimensions of the measurement volume, the particles are not in fact illuminated by a uniform plane wave. However, the effect of this is taken care of by the inclusion of the size dependence in J.

Figure 8 represents schematically a quadrant of the measurement volume function $J(x,z,d)$. It is shown as a monotonically decreasing function of x and

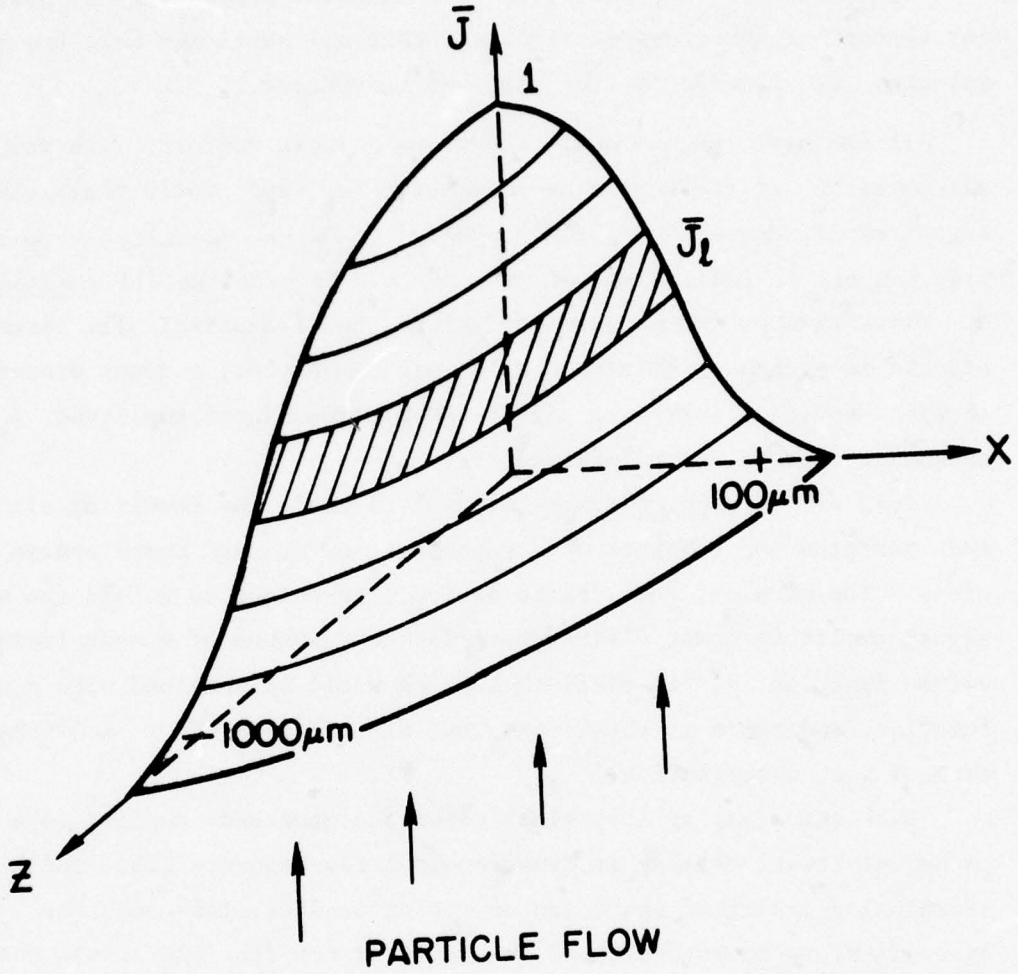

Figure 8. Schematic of a Quadrant of the Measurement Volume Function J(x,z,d)

z measured from the "center" of the measurement volume where it has its maximum value J_m. However, the following analysis is valid for more general forms of J.

It is assumed that particles have an equal probability of passing through any element of the cross-section, and that all particles have the same mean velocity U, irrespective of size and trajectory.

If the measurement volume function J were uniform, with value J_m, all particles of the same size parameter (α_k say) would yield the same signal amplitude $A_k = G(\lambda^2/4\pi^2)\, J_m F(\alpha_k)$ i.e. the quantity A would be a unique function of α, independent of x and z. In practice, if a monodisperse aerosol α_k flows through the measurement volume, and a statistically large number of signals is accumulated in the pulse height analyzer, a count distribution is obtained having a sharp cut off at the maximum signal amplitude A_k, and spreading down to lower amplitudes.

Further, if a polydisperse aerosol is used, the resulting signal amplitude distribution consists of a superposition of such monodisperse distributions. The problem, then, is to devise a technique to unfold the measured signal amplitude count distribution in the presence of a nonuniform measurement volume function J, to yield that which would be obtained with a uniform J function, and hence to obtain the true distribution of F and from this the aerosol size distribution.

Such unfolding or inversion techniques have been applied in a number of technical areas, notably in tomographic X-ray scanners [25], and have become technically practical since the advent of on-line mini-computers. Although a straightforward mathematical inversion is not feasible, given the experimental nature of the problem, efficient solution procedures have been developed for determining a solution which has an error magnitude of the same order as that of the measured input variables. Further, it is intuitively plausible that the more nearly the J function approaches the ideal rectangular form, the more accurate should be the inversion process. Thus there is an advantage in achieving a form for J that approaches the ideal rectangular one as closely as possible.

4.1 Formulation of Method

The problem is formulated as follows. First, it is convenient to normalize the functions J, F and A on their maximum values. Thus we define

$$\bar{J} = \frac{J}{J_m} \qquad (0 \le \bar{J} \le 1) \quad , \tag{4.3}$$

$$\bar{F} = \frac{F}{F_m} \qquad (0 \le \bar{F} \le 1) \quad , \tag{4.4}$$

where F_m is the maximum response function value corresponding to the largest particle in the aerosol of interest, or the largest size that it is of interest to measure.

The maximum signal value, corresponding to this maximum F value is then

$$A_m = G \frac{\lambda^2}{4\pi^2} J_m F_m \quad , \tag{4.5}$$

and we define

$$\bar{A} = \frac{A}{A_m} \qquad (0 \le \bar{A} \le 1) \quad , \tag{4.6}$$

Then (4.2) can be written in normalized form

$$\bar{A} = \bar{J} \bar{F} \tag{4.7}$$

Now, as is appropriate to the problem, we coarse-grain the functions $\bar{A}$, $\bar{F}$, treating them as discrete, rather than continuous variables, and let

$C(\bar{A}_i) \equiv C_i$ = Signal count rate for normalized signal peak amplitudes in the range $\bar{A}_i$ to $(\bar{A}_i + \Delta\bar{A}_i)$

$N(\bar{F}_j) \equiv N_j$ = concentration of particles in the size parameter range yielding normalized response function values in the range $\bar{F}_j$ to $(\bar{F}_j + \Delta\bar{F}_j)$

$\Delta S(\bar{A}_j, \bar{F}_j) \equiv \Delta S_{ij}$ = cross-sectional area of the measurement volume, normal to the flow direction, which yields normalized signal peak amplitudes in the range $\bar{A}_i$ to $(\bar{A}_i + \Delta\bar{A}_i)$ for particles having normalized response functions in the range $\bar{F}_j$ to $(\bar{F}_j + \Delta\bar{F}_j)$.

Then the count rate distribution is given by the equation set

$$C_1 = \sum_{j=1}^{m} U \Delta S_{1j} N_j$$

$$C_i = \sum_{j=1}^{m} U \Delta S_{ij} N_j \qquad (4.8)$$

$$C_m = \sum_{j=1}^{m} U \Delta S_{mj} N_j$$

which can be written more compactly in matrix form

$$\underline{C} = U \underline{\underline{\Delta S}} \cdot \underline{N} \qquad (4.9)$$

The subscripts i, j are written in order of increasing $\bar{A}$ and $\bar{F}$, starting with the smallest (utilized) amplitude channel ($i=1$) of the pulse height analyzer, and the smallest response function class ($j=1$) capable of recording a signal in that channel, and ending with the largest signal amplitude-class ($i=m$) and largest response function class ($j=m$) having non-zero values. The discrete classes are assumed contiguous, so that

$$\bar{A}_{i+1} = (\bar{A}_i + \Delta\bar{A}_i) \quad \text{and} \quad \bar{F}_{j+1} = (\bar{F}_j + \Delta\bar{F}_j) \qquad (4.10)$$

Hence m is the number of (utilized) channels in the pulse height analyzer and is also the number of response function classes into which the particle distribution is resolved. Here, and in what follows, it is assumed that $\bar{F}(\alpha)$ is monotonic, at least when coarse-grained over the intervals $\Delta\bar{F}_j$.

The signal amplitude classes $\bar{A}_i$ and the response function classes $\bar{F}_j$ are associated on a one to one basis through the choice

$$\bar{A}_k = \bar{J}_m \bar{F}_k \quad ,$$

or, since $\bar{J}_m = 1$ (4.11)

$$\bar{A}_k = \bar{F}_k$$

Since a particle yielding a response function in a given class $\bar{F}_j$ cannot give rise to a signal amplitude greater than $\bar{A}_j$, the cross-section matrix elements ΔS_{ij} are all zero for $i > j$. Thus Eqn. (4.9) can be written explicitly

$$\begin{vmatrix} C_1 \\ C_2 \\ C_3 \\ \vdots \\ C_i \\ \vdots \\ C_m \end{vmatrix} = \begin{Vmatrix} \Delta S_{11} & \Delta S_{12} & \Delta S_{13} \cdots \Delta S_{1i} \cdots \Delta S_{1m} \\ 0 & \Delta S_{22} & \Delta S_{23} \cdots \Delta S_{2i} \cdots \Delta S_{2m} \\ 0 & 0 & \Delta S_{33} \cdots \Delta S_{3i} \cdots \Delta S_{3m} \\ \vdots & \vdots & \vdots \quad \vdots \quad \vdots \\ 0 & 0 & 0 \cdots \Delta S_{ii} \cdots \Delta S_{im} \\ \vdots & \vdots & \vdots \quad \vdots \quad \vdots \\ 0 & 0 & 0 \cdots 0 \cdots \Delta S_{mm} \end{Vmatrix} \begin{vmatrix} N_1 \\ N_2 \\ N_3 \\ \vdots \\ N_i \\ \vdots \\ N_m \end{vmatrix} \qquad (4.12)$$

The inversion of Eqn. (4.12) is written symbolically

$$\underline{N} = \frac{1}{U} \underline{\underline{\Delta S}}^{-1} \cdot \underline{C} \qquad (4.13)$$

Given the count rate distribution of signal amplitudes $C_i(\bar{A}_i)$ in the pulse height analyzer channels, then <u>if</u> the ΔS matrix is known, Eqn. (4.13) can be solved to yield the distribution $N_j(\bar{F}_j)$ of normalized response functions. If the response function $F(\alpha)$ is known, either from computations (when the refractive index is known), or from a calibration experiment (see Section 5.0), the distribution of particle size parameters $N_j(\alpha_j)$ and hence the distribution of diameters $N_j(d_j)$ for the polydispersion can be obtained. The central problem is the determination of the cross-section matrix, to which we shall return shortly.

Up to this point the functional dependence of $\bar{A}_k(k)$ (and hence of $\bar{F}_k(k)$) has been arbitrary. Usually, pulse-height analyzers offer a choice of either a linear amplitude mode, for which $\bar{A}_{k+1} - \bar{A}_k = \Delta\bar{A}_k$ = constant for all k, or a logrithmic mode for which

$$\frac{\Delta \bar{A}_k}{\bar{A}_k} = \beta = \text{constant}$$

i.e.

$$\bar{A}_{k+1} = (1 + \beta)\, \bar{A}_k \qquad \text{(for all k)} \tag{4.14}$$

The constant β is chosen by setting the gain of the logarithmic amplifier to suit the relative size range of interest and the resolution i.e. the number of channels utilized.

The choice of the logarithmic mode is preferred for two reasons. First it is the most appropriate mode when dealing with particle distributions with a large relative spread. Second, as discussed below, in the case that $\bar{J}$ is independent of d, a condition that can effectively be realized in practice, a further simplification of the $\underline{\underline{\Delta S}}$ matrix results which reduces the number of independent elements from $m^2/2$ to m.

With a logarithmic mode, we also have in view of Eqn. (4.11)

$$\frac{\Delta \bar{F}_k}{\bar{F}_k} = \beta$$

i.e.

$$\bar{F}_{k+1} = (1 + \beta)\, \bar{F}_k \qquad \text{(for all k)} \tag{4.15}$$

4.2 Determination of the $\underline{\underline{\Delta S}}$ Matrix

Returning to the question of determining the $\underline{\underline{\Delta S}}$ matrix, in principle this can be deduced from measurements of the signal amplitude by traversing a single particle of known size d_j (e.g. attached to a microscope slide) through the measurement volume for a range of x, z and d.

Fortunately, a simpler, less tedious, and more direct procedure is available through the use of an aerosol generator capable of producing monodispersions of controlled size and concentration. The method proceeds as follows.

A monodisperse particle distribution $N(d_k)$ with a known diameter d_k and concentration N is passed through the measurement volume at a known mean velocity U. For a specified time the signals are accumulated in the pulse-height analyzer to yield the count rate distribution $C(\bar{A}_i) \equiv C_i$. Since $N(d_j) = 0$ for all j except $j = k$, the system of equations (23) reduces to a set of k equations of the form

$$C_i = U \, \Delta S_{ik} \, N_k \, , \tag{4.16}$$

which can be solved directly for the ΔS_{ik}. This yields the k elements in the kth column of the matrix. By repeating the procedure for different size classes k, successive columns of the $\underline{\underline{\Delta S}}$ matrix can be determined until, by m such measurements the whole $\underline{\underline{\Delta S}}$ matrix is known. Incidentally, in the process, the cut-offs of the count distributions at $\bar{A}_k$ yield an experimental calibration of the pulse height analyzer channel numbers in terms of the particle diameter (i.e. F(d)) for the particular refractive index employed.

This method has, in fact, been used and is satisfactory though time-consuming if m is large. In the process, however, it was realized that a much simpler technique is applicable under certain conditions, as follows.

When the amplitude response of the pulse-height analyzer is logarithmic, then if the transfer function for collection H, and hence the measurement function $\bar{J}$, is independent of d, it can be shown (Appendix II) that the ΔS matrix simplifies so that all the elements on any diagonal are equal. It can then be written

$$\underline{\underline{\Delta S}} = \begin{vmatrix} \Delta S_m & \Delta S_{m-1} & \Delta S_{m-2} & \cdots\cdots\cdots & \Delta S_2 & \Delta S_1 \\ 0 & \Delta S_m & \Delta S_{m-1} & \cdots\cdots\cdots & \Delta S_3 & \Delta S_2 \\ 0 & 0 & \Delta S_m & & \Delta S_4 & \Delta S_3 \\ 0 & 0 & 0 & & \vdots & \vdots \\ \vdots & & & \Delta S_m & \Delta S_{m-1} & \Delta S_{m-2} \\ & & & 0 & \Delta S_m & \Delta S_{m-1} \\ 0 & \cdots\cdots\cdots\cdots\cdots\cdots & & 0 & 0 & \Delta S_m \end{vmatrix} \tag{4.17}$$

In Eqn. (4.17), ΔS_ℓ is now the area in the x-z plane where the $\bar{J}$ function, which has been coarse-grained into logarithmic intervals with $\Delta\bar{J}_\ell/\bar{J}_\ell = \beta$, has the value $\bar{J}_\ell$ (Figure 9). Thus ΔS_m is the central area where $\bar{J}$ has its maximum value $\bar{J}_m = 1$. Also ΔS_1 is the peripheral area where the $\bar{J}$ function has its minimum coarse-grained value $\bar{J}_1 = 1/(1+\beta)^{m-1}$, such that a particle of the largest response function class $\bar{F}_m$ generates a signal falling in the smallest signal amplitude class $\bar{A}_1$.

The significance of this simplification is that now all the matrix elements can be determined from a single calibration using monodisperse particles of the largest size class of interest, from the equation set

$$C_i = U \Delta S_\ell N_m , \quad \ell = 1,m \tag{4.18}$$

The calibration procedure is then particularly simple and quick.

Experimental evidence for the fact that the J-function is sensibly independent of d, at least for the conditions of the experiment, is adduced in Section 5.0, and hence justifies the use of this simple calibration procedure.

One further point concerning the calibration technique should be discussed. To determine the absolute values of the ΔS_i from Eqn. (4.18) it is necessary to know both the velocity U and the absolute concentration N_m. In practice, when using the monodisperse particle generator, it is not an easy matter to determine the absolute concentration at the measurement station. Even if the particle generation rate is known, it is difficult to allow for loss of particles by deposition in the feed tube.

If only the relative size-concentration distribution of an unknown aerosol is required, then relative values of the ΔS_ℓ suffice, and these can be determined without knowing either U or N_m absolutely. When an absolute calibration is required the concentration N_m can be determined by an extension of the basic calibration technique as described below.

In performing the calibration procedure based on the use of Eqn. (4.18) the total count rate in channels $i = \ell$ to m is

$$\sum_{i=\ell}^{m} C_i = U \sum_{i=\ell}^{m} \Delta S_i \; N_m \tag{4.19}$$

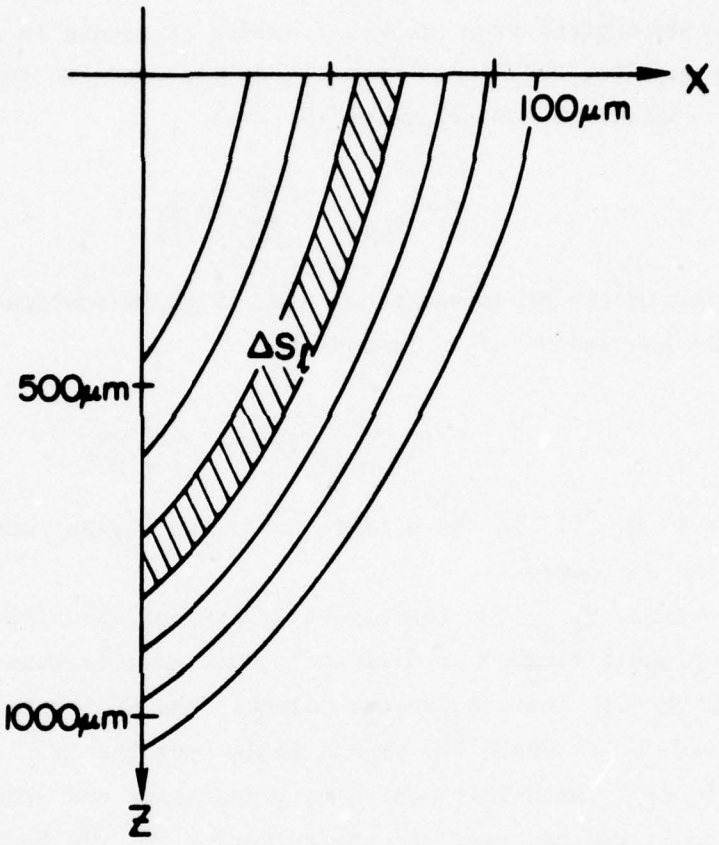

Figure 9. Schematic of ΔS_ℓ Corresponding to $\overline{J}_\ell$ of Figure 8

which we write

$$C_{\ell,m} = U S_{\ell,m} N_m \tag{4.20}$$

$C_{\ell,m}$ is determined from the total number of counts in channels ℓ to m in a known time, and if the velocity is measured, we can determine N_m from (4.20) provided we can determine the area

$$S_{\ell,m} \equiv \sum_{i=\ell}^{m} \Delta S_i \tag{4.21}$$

The latter is the cross-sectional area of the measurement volume which has $\bar{J}$ values bounded by $\bar{J}_m = 1$ and

$$\bar{J}_\ell = \frac{1}{(1+\beta)^{m-\ell}} = \frac{1}{(1+\beta)^r} \tag{4.22}$$

where $r = (m - \ell)$ is the difference in the channel numbers over which the count rate is summed.

The area $S_{\ell,m}$ can readily be determined experimentally by traversing a small pinhole (e.g. 5 μm diameter), much smaller than the detection aperture pinhole, through the measurement volume. The extent in x and z of the cross-section for which the signal falls from the m^{th} channel (at the center) to the $(m-r)^{th}$ channel is mapped out, and hence the area is found.

In this way the absolute concentration N_m is found from Eqn. (4.20) and then the absolute values of the ΔS_i are found from Eqn. (4.18). The use of this method with monodispersions of different size, to check experimentally that $\bar{J}$ is indeed not a function of d, is discussed in Section 5.0.

4.3 Implementation of Inversion Technique

Once the ΔS_ℓ matrix elements are determined from such a calibration, they are entered in the matrix inversion algorithm of a mini-computer. Then, for an aerosol under investigation, the count rate distribution C_i from various channels of the pulse height analyzer are automatically entered into the computer. It is useful, however, to observe the data on the instrument's visual display as a check on correct functioning.

Because of the experimental uncertainty in determining $\underline{C}$ and $\underline{\underline{\Delta S}}$, the problem $N = (U\ \underline{\underline{\Delta S}})^{-1}\ \underline{C}$ cannot be accurately solved by straightforward matrix inversion techniques. Instead, the solution $\underline{N}$ is derived by searching for a non-negative vector $\underline{N}$ which minimizes the residual vector $R = \underline{C} - U\ \underline{\underline{\Delta S}}\ \underline{N}$. A satisfactory solution to this problem was found through use of a non-negative least squares (NNLS) solution procedure developed by Lawson and Hanson [26]. This procedure minimizes error propagation and also outputs values of residuals R_j which allows one to judge the accuracy of the resulting N_j distribution.

5.0 EXPERIMENTAL RESULTS

The objectives of this section are two-fold:

1. Compare experimental results for the scattering response function F(d) with the calculations of Section 2.
2. Validate the accuracy of the inversion scheme described in Section 4.

The most direct method of validating the approach described up to this point consists of measuring well-characterized monodispersions of known size and concentration by using a Berglund-Liu monodisperse particle generator [27]. Such a device is claimed to generate particles within ±1% of the stated diameter. Microscopic examination of samples collected on glass slides confirm monodispersity to within the ±5% resolution of a microscope graticule. Spherical droplets are generated from oleic acid which has a refractive index of $\tilde{n} = 1.46 + 0.0i$, i.e. negligible absorption.

For a given nozzle diameter (20 μm, 10 μm, or 5 μm), a 10:1 range of particle sizes can be generated by varying the percentage of oleic acid in isopropyl alcohol. The alcohol evaporates in a long residence time drying chamber leaving oleic acid droplets with diameters proportional to $C^{1/3}$, where C is the oleic acid concentration. The present experiments used the 20 μm nozzle to generate particles in the range 2.5 μm to 25 μm. The other nozzles (10 μm and 5 μm) can be used to generate particles down to 0.5 μm.

Experimental values of F(d) are derived from the set of curves shown in Figure 10. Each curve corresponds to the PHA data generated for a known particle size. The relative scattering response for each size is given by the threshold channel where the number count increases sharply. In practice, there exist a few doublets and triplets of the primary particle size produced by the particle generator. Thus the threshold channel is taken as that channel where the number count is 10% of the peak number count. Comparison of these experimental results and the calculations of F(d) in Section 4 are shown in Figure 11. These results indicate that scattering theory is quite adequate for the range of conditions investigated, although further work is necessary to confirm the extent of the resonances or multi-valued regions of the response function.

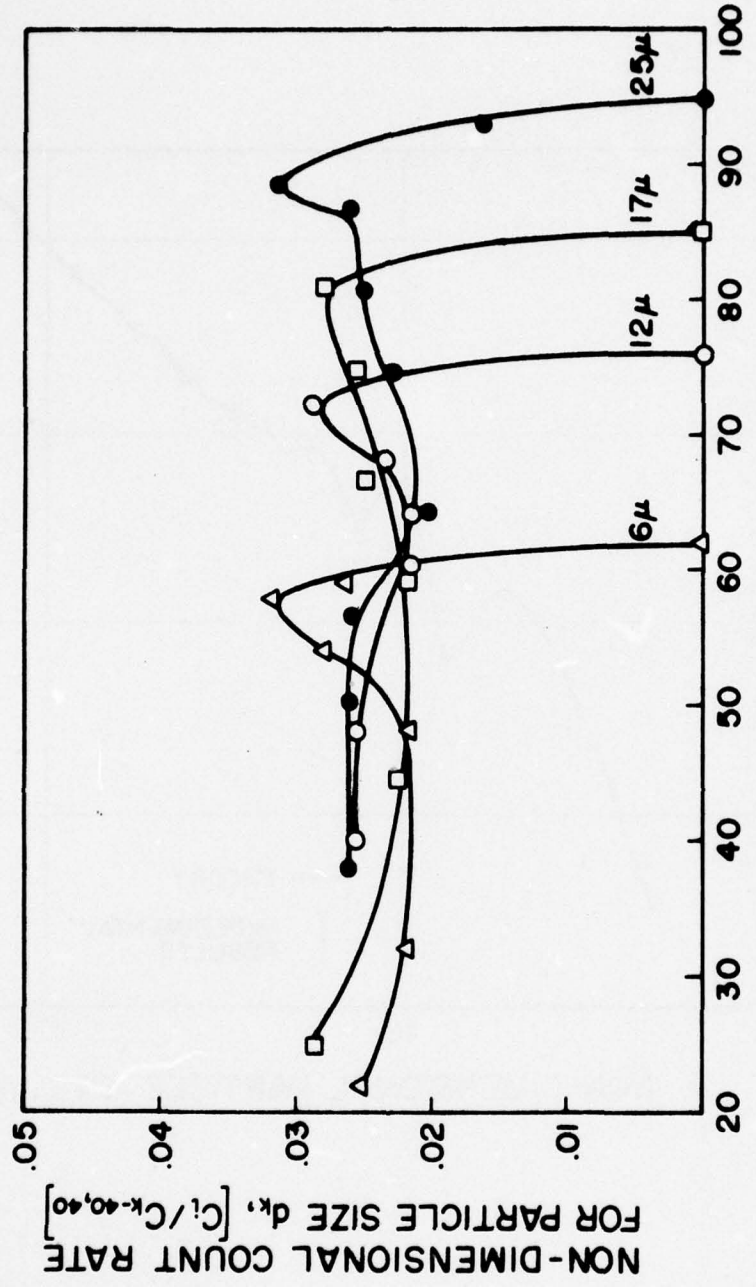

Figure 10. Non-Dimensional Count Rate Vs Pulse Height Analyzer Channel Number for Particle Sizes d_k = 6,12,17,25 μm

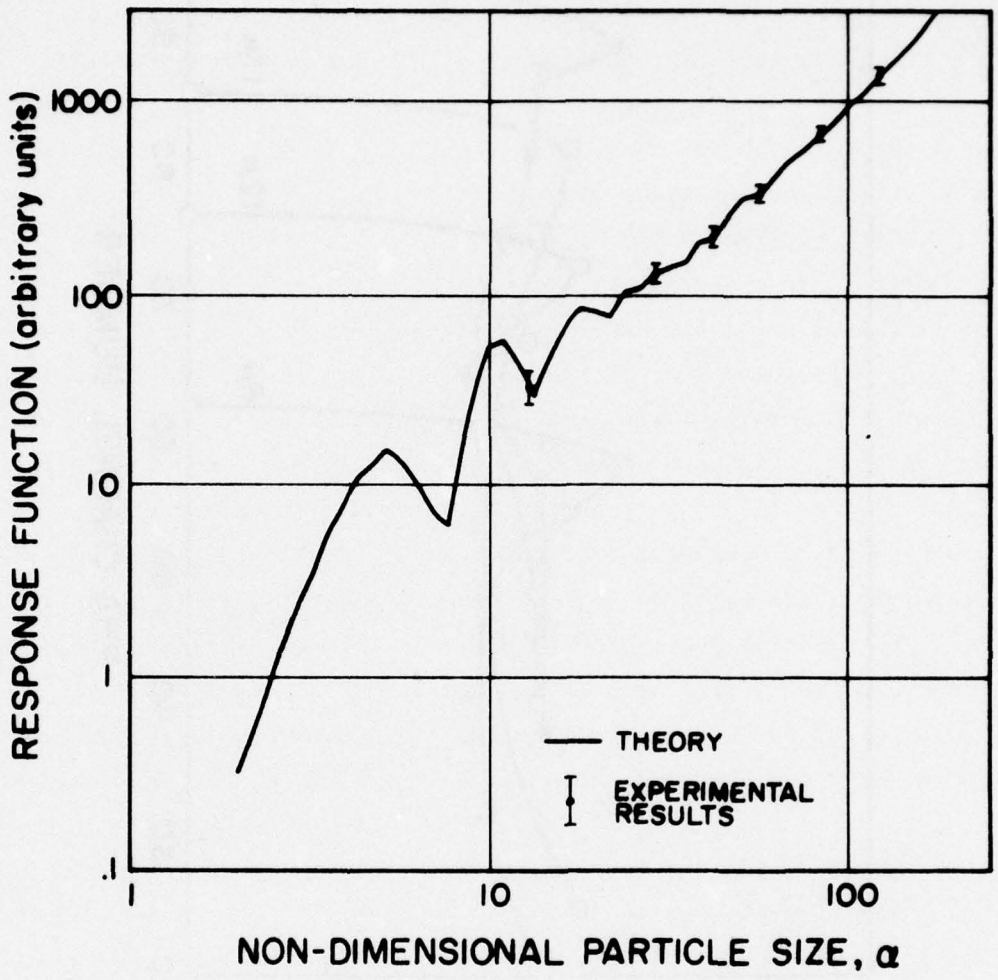

Figure 11. Experimental Results for Oleic Acid Particles Compared with Theoretical Response Function F(d)

Ignoring the resonances and taking a mean curve fit in the range of 2 - 30 μm gives an approximate scattering function dependence on particle size as $F(d) \alpha d^{1.65}$ which is similar to the power dependence of the Royco PC 215 and PC 245 particle counters where the exponent ranges from 1.5 to 1.8 [12]. This result is to be expected since light collection geometries for these devices are similar and the effect of a polychromatic illumination is only one of smoothing the resonances. Further work is continuing to generate particles in the .5 - 2 μm range and thus provide a check on the response curve for small particles.

Proof of numerical inversion accuracy requires knowledge of calibration source particle number density along with particle size. The number of particles produced by the particle generator was 90,000/sec and the the flow conditions used in our experiments gave a maximum number density of 108 particles/cm^3. However, a flexible hose was used to convey the particles from the generator to the measurement volume and in the process a significant fraction of particles was lost to the hose wall. In addition it is possible that the local number density traversing the measurement volume may not correspond to the bulk mean number density at the hose exit, even were it known. Consequently we use the method described in the latter part of Appendix II to determine the local number density. It is clear that every particle above the minimum size threshold traversing the measurement cross-section S_r will be counted, as long as coincidence errors do not occur. For the experimental conditions mentioned, coincidence errors are negligible. The local number density can be directly evaluated for a monodispersion by the formula (Eqn. II.8).

$$N_k = \frac{C_{k-r,k}}{U \cdot S_{k-r,k}}$$

where $C_{k-r,k}$ is the total number of particle counts from channel (k-r) to k where r corresponds to $\bar{A}_{k-r}/\bar{A}_k = 0.1$ or from Eqn. II.1, $r = 2.3/\beta$ for $\beta < 0.2$.

In general $S_{k-r,k}$ is a function of particle size and Table 5.1 summarizes values of $S_{k-r,k}$ for several pinhole diameters and two values of $\bar{A}_{k-r}/\bar{A}_k$.

Table 5.1. Variation of Measurement Volume Cross-Section, $S_{k-r,k}$, With Pinhole Diameter, d_k, and Amplitude Reference Level $\bar{A}_{k-r}/\bar{A}_k$

Pinhole Diameter, d_k	$S_{k-r,k}$ $\left[(cm^2)\right]$	
	$\bar{A}_{k-r}/\bar{A}_k = e^{-1}$	$\bar{A}_{k-r}/\bar{A}_k = .1$
5 μm	.00525	.00115
12.5 μm	--	.0011
25 μm	.0045	.00102

The values of $S_{k-r,r}$ are the same for the 5 μm and 12.5 μm pinholes while $S_{k-r,r}$ decreases by 11% for the 25 μm pinhole. Thus for particles < 25 μm diameter $S_{k-r,r} \approx S_r$ and is sensibly independent of particle size. Given that S_r is reasonably constant, from Appendix II, Equation II.13, we have $\Delta S_{m-(k-i)}/S_{k-r,r} = C_i/C_{k-r,r}$ and thus the normalized cross sections can be derived directly from the PHA number amplitude spectrum C_i, i = 1, m. Figure 12 shows a plot of normalized cross section calibrations for five particle diameters ranging from 6 μm to 25 μm.

A mean curve can be drawn through all the calibration points which is within ± 10% of all values for the five particle sizes, indicating that the normalized values of the cross section matrix are sensibly independent of particle diameter up to 25 μm. Coupling this result with $\Delta S_{k-r,r} \approx$ constant up to 25 μm we conclude that the cross section elements are reasonably independent of particle size up to 25 μm for our instrument geometry.

We know that the beam intensity is similar for other overall beam dimensions (Eqn. 2.2) and thus we can generalize the above results to say that the particle size should be smaller than ~ 35% of the 1/e beam width for the diagonal elements of $\underline{\underline{\Delta S}}$ to be identical.

The final and essential test of the inversion scheme and its accuracy is to obtain data on an aerosol of known particle size distribution. A mixed aerosol of known particle sizes was obtained by sequentially adding and storing the data from four monodisperse aerosols generated by the Berglund-Liu particle generator. This accumulated data is shown in Figure 13, which represents the raw PHA data generated by a mixture of 6, 12, 17 and

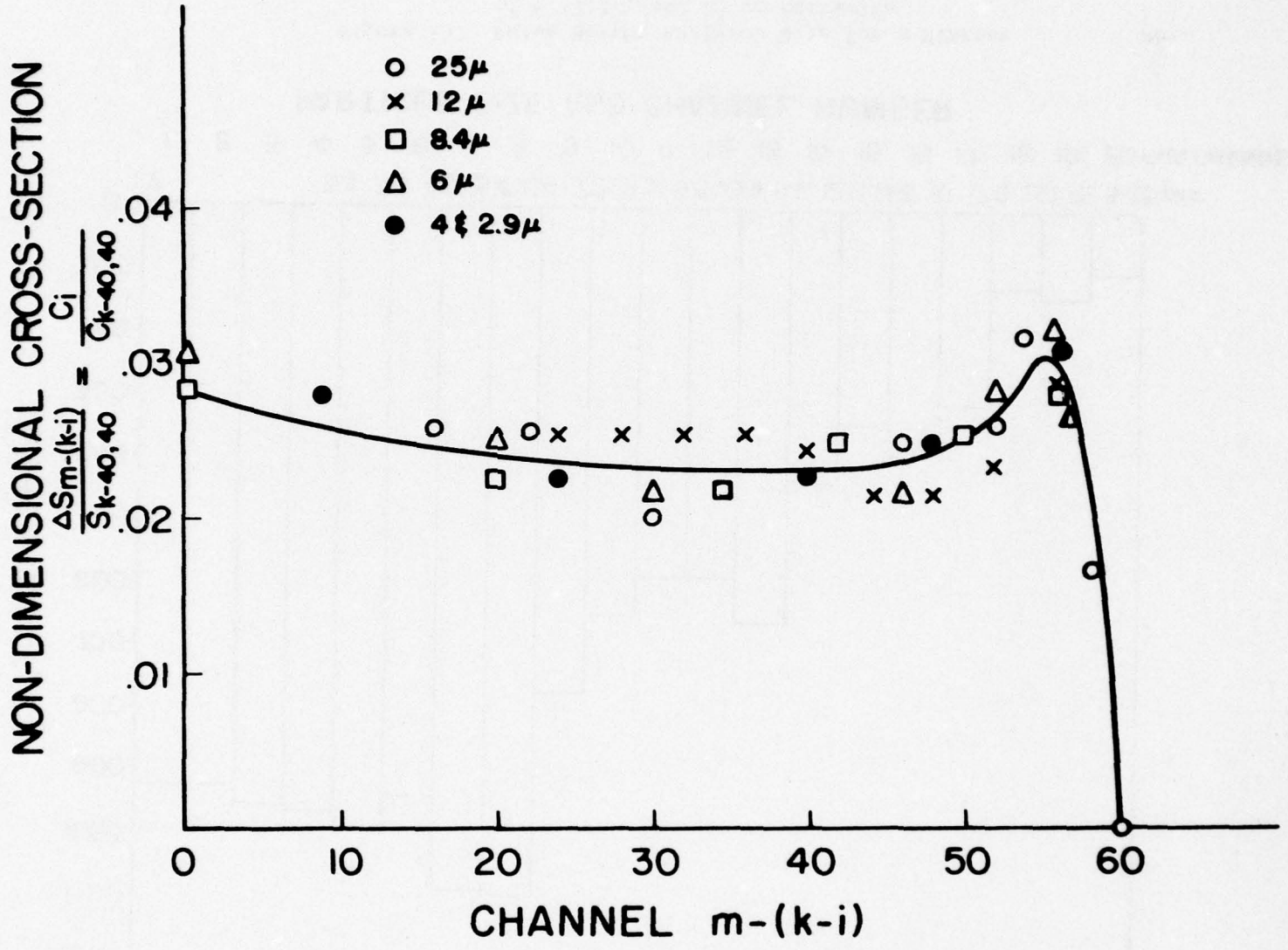

Figure 12. Non-Dimensional Cross-Section Calibration Results for Particle Sizes Ranging from 2.9 - 25 μm

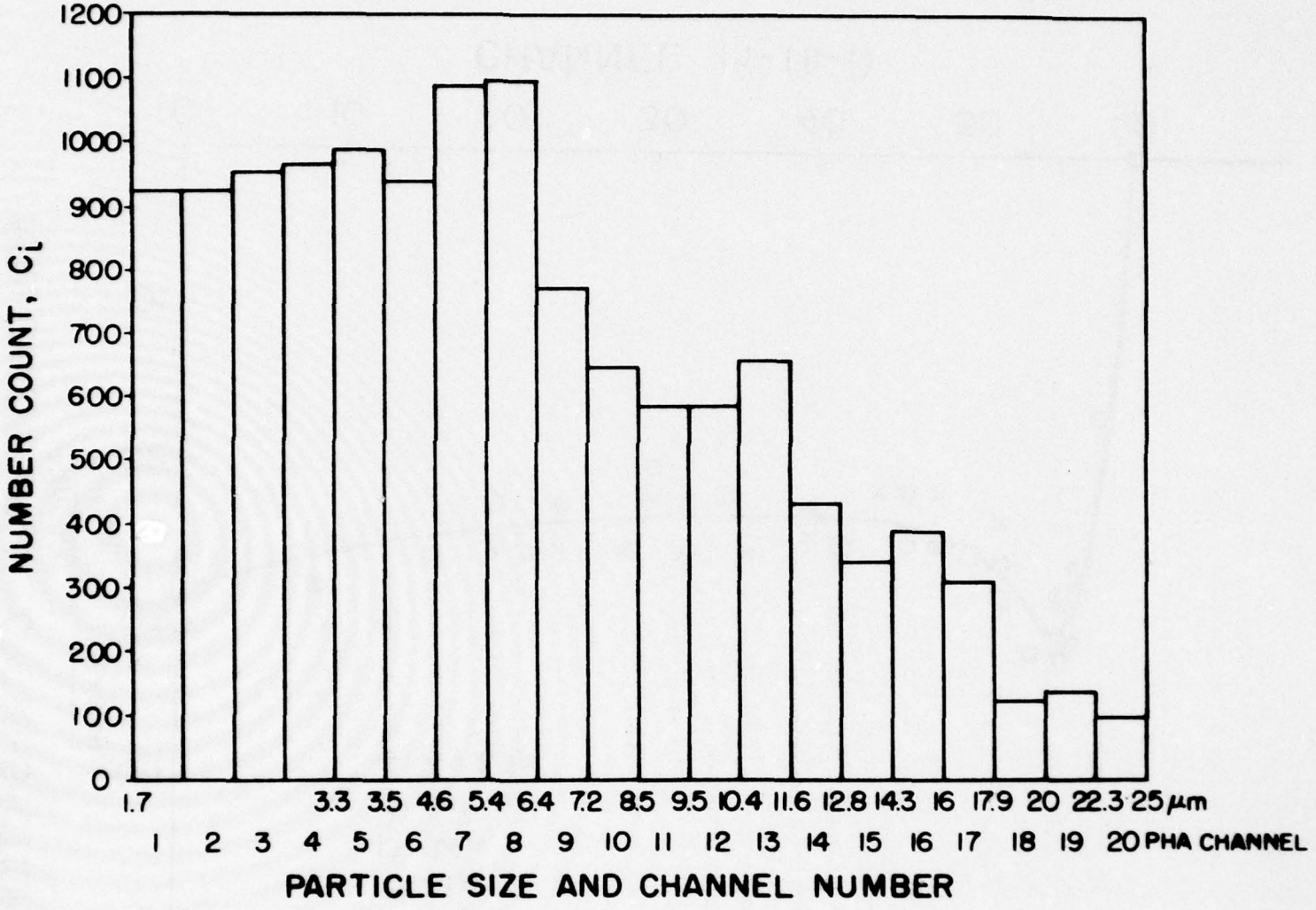

Figure 13. Pulse Height Analyzer Data for a Mixture of 6,12,17, and 25 μm Particles

25 μm particles. Although the PHA has a total of 100 amplitude channels giving $\beta = .06$, the data was 'compressed' by a factor of three to minimize computation time. The 'compressed' channel width (β) is equal to 0.21 which corresponds to a particle diameter resolution of $\Delta d_k/d_k \approx 0.13$. Application of the inversion scheme, (Eqn. 4.13), gives the results shown in Figure 14. The four major particle size peaks occur within ±10% of the known particle diameters although a small spurious peak occurs at channel 11. The peak at channel 11 represents a 10% error in number count and is consistent with the accuracy of the cross section calibration curve (Figure 12).

An approximate analysis of error propagation in the inversion scheme due to uncertainties in measurements of C_i and $\underline{\underline{\Delta S}}$ is presented in Appendix III. The results of the error analysis show that the upper bound uncertainty in N_i varies from ±13% in channel 9 to ±26% in channel 20. Higher counting rates for practical aerosol flows should reduce these uncertainties.

It should be remembered that the generated number density is 108 cm^{-3} (an upper bound) which is to be compared to the computed values shown in Figure 12. The actual number densities at the nozzle exit of the particle generator decrease with increasing particle size, consistent with observed increases in particle deposition with increasing particle size [28]. The computed values in Figure 14 are also consistent with individual particle size calibration tests, Table 5.2, where the number density was calculated according to Eqn. 4.20.

Table 5.2. Comparison of Number Density Results for Figure 12 and Calibrations.

Particle Size (μm)	Number Density, N_m (cm^{-3})	
	Calibration	Fig. 12 Results
6	73	93
12	77	66
17	63	57
25	27	31

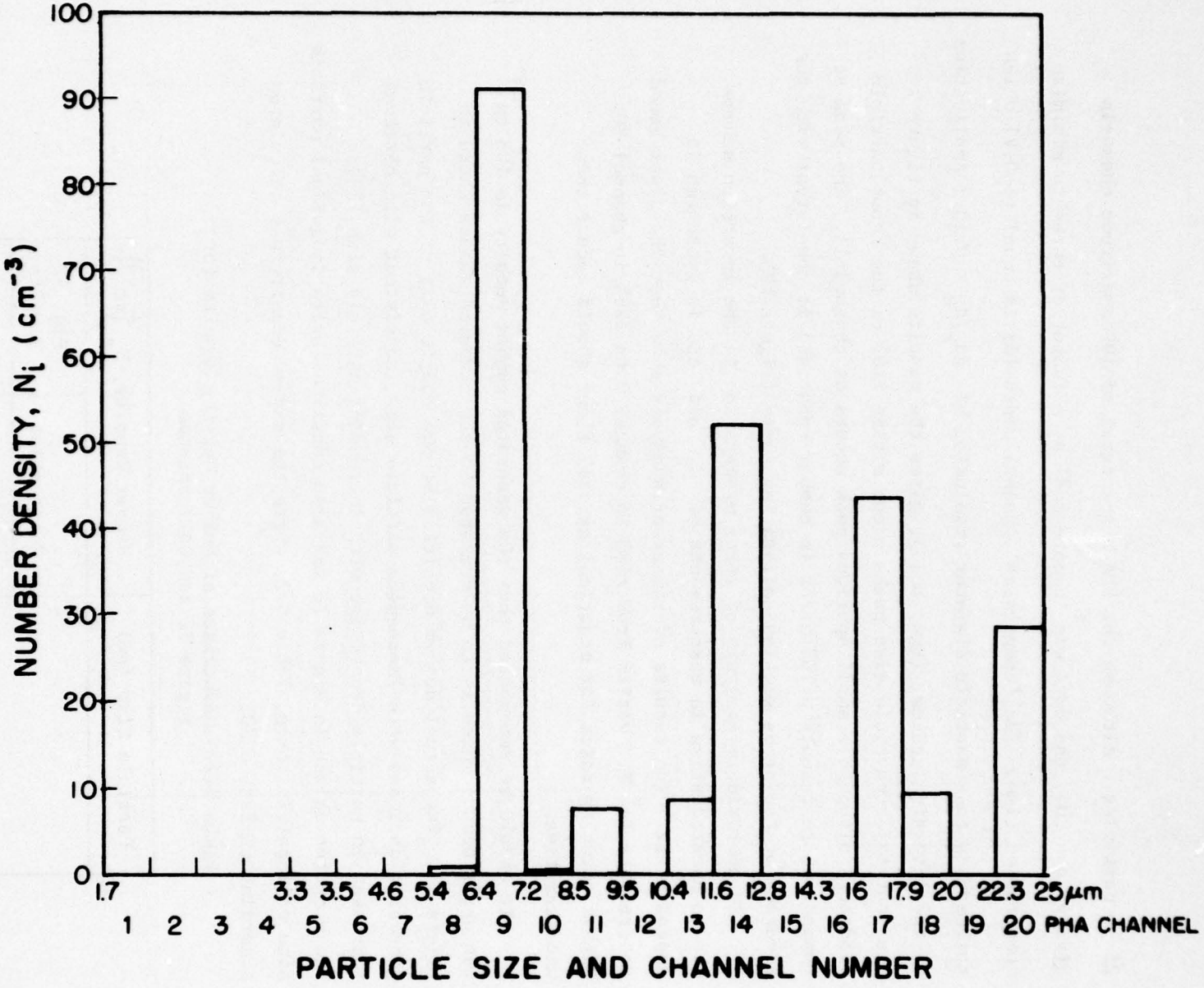

Figure 14. Number Distribution Results Following Application of Eqn. 4.13 to the Data of Figure 13

The 'calibration' number densities also generally decrease with increasing particle size although exact correspondence of the number density with the calibration tests was not found because the deposition rates and thus actual number density at the nozzle exit are very sensitive to particle feed line curvature which was not carefully controlled in different tests.

6.0 DISCUSSION AND CONCLUSIONS

The in situ particle sizing counter described herein satisfies the principal practical requirements of such an instrument for many important applications. The optical access requirements are modest and can be readily satisfied for laboratory scale flow systems. Particles can be sized over at least a 10:1 diameter range with a resolution $\Delta d/d \leq 0.15$, which is adequate for most aerosols of interest. The instrument has been conclusively demonstrated as capable of resolving the structure of a polydispersion consisting of several superimposed monodispersions in the range 2.5-25 μm. By adjusting the instrumental geometry, it should be straightforward to deal with sizes ranging up to ~100 μm. The extension to sizes $\lesssim$ 2 μm appears possible but requires further work to resolve the limitations set by the first resonance in the scattering function which typically occurs in the range of 1 μm. Another important feature is that the measurement volume can be made small enough to allow measurements with high particle concentrations, in the range of interest for most applications.

The key feature of the method is the use of a computer-based inversion scheme which allows one to unfold the effect of the random trajectory dependence of the scattered signals together with a straightforward calibration technique which gives the necessary information on the scattering function F(d) and the matrix elemental areas ΔS_{ij} required for the inversion.

Although the experimental work was based on the use of non-absorbing spherical droplets supplied from a monodisperse particle generator, the method should also be applicable to absorbing and irregular particles. For absorbing spherical particles of known refractive index, Mie scattering computations can be used as a guide, but if the refractive index is unknown, or the particles are irregular, the calibration technique can always be used provided it is possible to obtain monodespersions of the aerosol of interest.

Such an approach has been described recently by Marple and Rubow[29,30], with application to irregular absorbing particles such as pulverized coal, road dust and other aerosols. They used a two-stage impactor to produce a

sharp upper cutoff in particle size for the aerosol of interest. This was then fed to a sampling type optical counter (Royco 218) to give a single calibration point. By using different nozzles in the impactor a series of calibration points for different aerodynamic diameters was obtained. Figure 15 shows their results for a variety of aerosols. It may be noted that a mean calibration curve could be used for all of these aerosols without introducing a size error of more than ±30%. This is an encouraging result for application of optical sizing to various irregular and absorbing aerosols of practical interest. This calibration technique using an impactor is directly applicable to the present in situ instrument for measurement on irregular and absorbing particles.

In the future it is planned to explore this method with the present in situ instrument to determine the size distributions of fly ash particles in a cold flow electrostatic precipitator dust tunnel.

Another potential area of application of the present instrument is to sizing particles in hot systems, such as liquid spray combustors and pulverized coal combustion systems. Two potential problems may be anticipated in hot systems, namely interference from background thermal radiation and beam and image wander due to fluctuating refractive index inhomogeneities. Estimates of the effect of the thermal background show that this should be negligible for sizes down to 0.5 μm if a laser line filter of 20Å width is employed. The effect of beam wander is more difficult to estimate and depends on the amplitude of thermal gradient fluctuations expected in a particular flow system. It is planned to study such effects by making measurements in a small burner system.

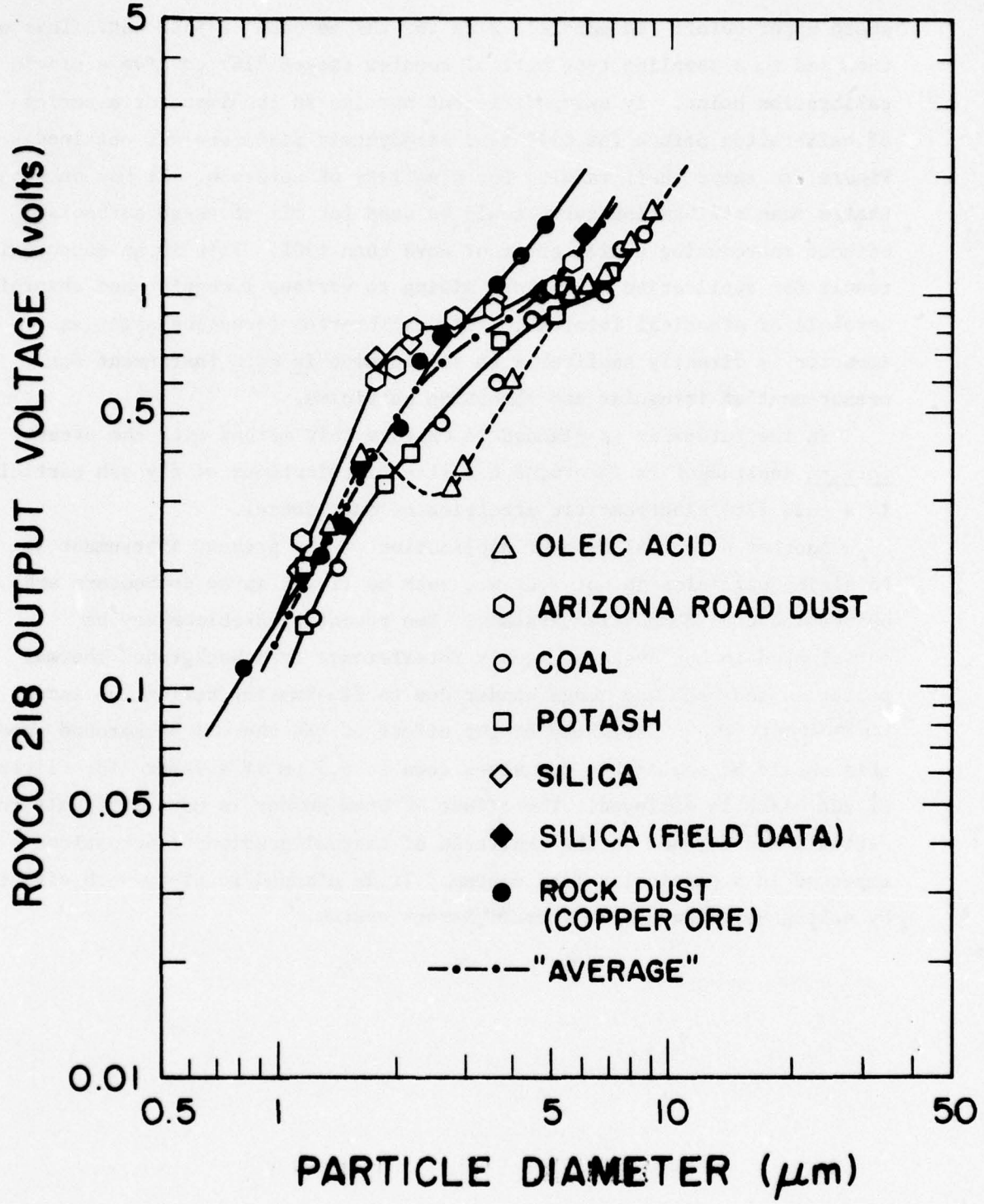

Figure 15. Response Curves for a Variety of Aerosols (Absorbing and Nonabsorbing) Using a Royco Forward Scatter Counter

ACKNOWLEDGEMENTS

Our thanks are due to Li Shing Cheng who performed the numerical calculations, and to Philip Krug for his enthusiastic work on the electronics and software. Informative discussions with Al Lieberman and Art Bates of Royco Instruments and Takashi Nakamura of the High Temperature Gas Dynamics Laboratory are gratefully acknowledged.

APPENDIX I SIGNAL COINCIDENCE EFFECTS

For a given aerosol size distribution and instrumental size range, there is a limit to the concentration that can be measured set by the occurrence of interference. The latter can be defined as occurring when the signal due to one particle is significantly enhanced by signals due to other particles present in the measurement volume "simultaneously", i.e., within the resolving time τ of the electronics. Clearly, interference is most likely to be a problem for the measurement of the smallest particles in the distribution.

Consider a polydispersion of given relative size distribution $(N_j(d_j)/\sum N_j)$, and suppose the instrument is set up so that the maximum size class (d_{max}) of particle will register signals in the maximum amplitude channel A_m of the pulse height analyzer, while the lowest amplitude channel A_1 just registers signals from the smallest size class (d_{min}) it is required to measure. We wish to derive criteria for how large the total concentration $\sum N_j$ can be without the occurence of significant interference.

For simplicity, we take this to be the condition that the probability of a signal from the smallest size class (1) (strictly the smallest scattering amplitude class) being overlaid by <u>one or more</u> additional signals of equal or larger amplitude is less than some critical value (say $\leq$ 20%). Since a simultaneous signal in any amplitude class i = 1 to m will cause such interference, and because the events are statistically independent, the required conditional probability is just the probability that one or more signals is present in any of the channels during the resolving time τ.

Now the average total rate of signals is $\sum_{i=1}^{m} C_i$, and the probability of n signals being present simultaneously is given by the Poisson distribution

$$P(n,x) \equiv \frac{x^n(\exp -x)}{n!} \qquad (I.1)$$

where

$$x \equiv \sum_{i=1}^{m} C_i \, \tau$$

Hence the probability of one or more signals being simultaneously present is $1 - P(0,x) = 1 - \exp(-x)$, and the required probability of interference is

$$P_{int} = 1 - \exp -\left(\sum_{i=1}^{m} C_i \tau\right). \tag{I.2}$$

Since we require that P_{int} is small, we can approximate (I.2) by

$$P_{int} \approx \sum_{i=1}^{m} C_i \tau. \tag{I.3}$$

Now, from Eqn. 4.8, we have

$$\begin{aligned} \sum_{i=1}^{m} C_i &= U \left\{ N_1 \Delta S_m + N_2 (\Delta S_m + \Delta S_{m-1}) + - - \right. \\ &\qquad \left. + N_m (\Delta S_m + --- + \Delta S_1) \right\} \\ &= U \sum_{j=1}^{m} N_j \sum_{\ell=m-j+1}^{m} \Delta S_\ell = U \sum_{j=1}^{m} N_j \, S_{(m-j+1),m} \end{aligned} \tag{I.4}$$

Here

$$P_{int} = U\tau \sum_{j=1}^{m} N_j \, S_{(m-j+1),m} \tag{I.5}$$

This shows that the larger particles in the distribution have a higher weight for causing interference because there are more channels in which they are capable of recording interfering signals. Equivalently, the larger particles experience a larger measurement volume ($\propto S_{(m-j+1),m}$), and hence have a larger probability of detection. It is also clear that the probability of interference depends on the shape of the distribution as well as the total concentration.

In Section 5 it was shown that for a Gaussian beam profile and a logarithmic amplitude mode of the pulse height analyzer, the incremental areas ΔS_ℓ are approximately constant, independent of ℓ, so that

$$S_{(m-j+1),m} \approx \sum_{\ell=m-j+1}^{m} \Delta S_\ell = j \, \Delta S \tag{I.6}$$

and

$$P_{int} \approx U\tau\ \Delta S \sum_{j=1}^{m} j\ N_j \tag{I.7}$$

This can be expressed in terms of the effective measurement volume as follows. Assuming that the resolution time τ is equal to the transit time U/L, where the length L of the measurement-volume in the flow direction is set by the pinhole diameter in the collection of optics, Eqn. (I.7) can be written

$$P_{int} \approx V_m \sum_{j=1}^{m} \left(\frac{j}{m}\right) N_j \tag{I.8}$$

where

$$V_m = L\ S_m \approx Lm\ \Delta S \tag{I.9}$$

is the effective (maximum) measurement volume. Eqn.(I.8) can be written

$$P_{int} \approx V_m\ N_T \left(\frac{\bar{j}}{m}\right) \tag{I.9}$$

where

$$N_T = \sum_{j=1}^{m} N_j \tag{I.10}$$

is the total concentration over the size range being measured, and

$$\bar{j} = \frac{\sum_{j-1}^{m} j\ N_j}{\sum_{j-1}^{m} N_j} \tag{I.11}$$

is the average channel number determined by the weight of the distribution N_j.

Equation (I.11) shows that the maximum total concentration that can be measured without significant interference is determined by the product of two factors, V_m and $(\bar{j}/m)$ which we discuss in turn.

The effective measurement volume V_m depends on two factors: first, the optical geometry determined by the waist diameter of the laser beam and by the F number, collection angle Θ_c and the pinhole diameter of the collection optics; second, by the size range (d_{max}/d_{min}) to be measured, as it determines the range of scattering amplitudes F_m/F_1 and hence signal amplitudes

A_m/A_1 to be accommodated. If S_r is the experimentally determined reference area, inside the contour where $\bar{J} = 1/e$, and if the response function is approximated by $F \propto d^p$ (where $p \approx 1.65$ for our experimental conditions), then we may write for the effective maximum measurement cross-section

$$S_m = p\, S_R\, \ell n\, (d_{max}/d_{min}) \tag{I.12}$$

In practice, the optical geometry is chosen to suit the maximum particle diameter to be measured. For instance, for $d_{max} \sim 25$ μm, the geometry used to obtain the results reported in Section 5 resulted in a reference area $S_R \sim 4\text{x}10^{-4}$ cm^2, i.e. approximately $60\, d_{max}^2$. With $p = 1.65$ and $(d_{max}/d_{min}) = 10$, together with $L = 100$ μm, we find an effective measurement volume of $V_m \sim 1.5\text{x}10^{-5}$ cm^3.

The second factor $(\bar{j}/m)$ is determined by the particle distribution function. Its minimum value is $(\bar{j}/m) = (1/m)$ when the distribution is strongly peaked in the smallest-channel. Thus the lower bound of P_{int} is $V_m\, N_T/m$. For measurement of sizes greater than the mode (maximum) of the concentration distribution, we consider distributions of the form

$$N(d) = k\, d^{-q} \tag{I.13}$$

where q is positive. This yields

$$N_j = \int_{d_j}^{d_j+\Delta d_j} N(d)\, \delta d \approx \frac{k\, \Delta d_j}{d_j^{\,q}} . \tag{I.14}$$

For $F \propto d^p$, we have

$$\Delta d_j \approx (\beta/p)\, d_j , \tag{I.15}$$

hence

$$N_j \approx \frac{k\, (\beta/p)}{d_j^{\,q-1}} . \tag{I.16}$$

In the special case $q = 1$, we have

$$N_j = k\, (\beta/p) = \text{constant},$$

$$\bar{j} = \frac{1}{m} \sum_{j=1}^{m} j = \frac{(m+1)}{2}, \tag{I.17}$$

and for $m >> 1$, $P_{int} \approx V_m N_T/2$.

In practice, most distributions decrease more rapidly than d^{-1}. For instance for d greater than the mode of the distribution by mass, $q > 3$. This weights $\bar{j}$ to values lower than $m/2$, and reduces the probability of interference.

In general for $N \propto d^{-q}$, we have

$$N_j \approx \frac{k\ (\beta/p)}{d_{min}^{(q-1)}\ (d_{max}/d_{min})^{(j-1)(q-1)/(m-1)}}. \tag{I.18}$$

This yields

$$\bar{j} \approx \frac{1}{\left[(d_{max}/d_{min})^{(q-1)/(m-1)} - 1\right]} + \frac{\left[(d_{max}/d_{min})^{(q-1)} - (m+1)\right]}{\left[(d_{max}/d_{min})^{(q-1)} - 1\right]}. \tag{I.19}$$

For $\left[(d_{max}/d_{min})^{(q-1)/(m-1)} - 1\right] \ll 1$, and

$(d_{max}/d_{min})^{(q-1)} \geq m$, this reduces to

$$\bar{j} \approx \frac{(m-1)}{(q-1)\ \ell n\ (d_{max}/d_{min})} \tag{I.19}$$

which shows that, under these conditions, the factor $(\bar{j}/m)$ is less than (0.5) and decreases as the distribution falls more rapidly, as $1/(q-1)$. Combining (I.19) with (I.12) then leads to

$$P_{int} \approx \frac{p}{(q-1)} L S_R N_T \approx \frac{p V_R N_T}{(q-1)} \tag{I.20}$$

Specifically, for $(d_{max}/d_{min}) = 10$, $m = 20$ and for $q=1,2,3,4$ we have $(\bar{j}/m) = 0.53$, 0.33, and 0.22 and 0.16 respectively. Thus the factor $(\bar{j}/m)$ decreases rather slowly as q increases.

In particular, for the instrumental conditions reported in Section 5, for which $V_m \approx 1.5 \times 10^{-5}$ cm^3, and taking $P_{int} = 0.2$, we find for the maximum concentration $N_T \sim 4 \times 10^4$ cm^{-3} for $q = 2$ and $N_T \sim 6 \times 10^4$ cm^{-3} for $q = 3$.

For $d_{max} = 25$ μm, and a particle specific gravity of 2, these dispersions correspond respectively to mass concentrations of 30 and 20 grams/m^3, which are rather higher than the fly ash loadings at the exhaust of pulverized coal combustors.

APPENDIX II CONDITIONS FOR IDENTITY OF DIAGONAL ELEMENTS OF $\underline{\underline{\Delta S}}$

With the choice of a logarithmic response on the pulse-height analyzer we have from Eqs (4.10), (4.11) and (4.14) the relations

$$\left.\begin{aligned} &\bar{A}_{k+1} = (1+\beta)\,\bar{A}_k = \bar{F}_{k+1} = (1+\beta)\,\bar{F}_k \\ \text{and}\quad &\frac{\Delta\bar{A}_k}{\bar{A}_k} = \frac{\Delta\bar{F}_k}{\bar{F}_k} = \beta \end{aligned}\right\} \qquad \text{(II.1)}$$

valid for all k. To be consistent with Eqn. 4.7, $\bar{J}$ is coarse grained into levels $\bar{J}_\ell$ $(1 \le \ell \le m)$ such that

$$\left.\begin{aligned} &\bar{J}_{\ell+1} = (\bar{J}_\ell + \Delta\bar{J}_\ell) = (1+\beta)\,\bar{J}_\ell \\ \text{and}\quad &\frac{\Delta\bar{J}_\ell}{J_\ell} = \beta \end{aligned}\right\} \qquad \text{(II.2)}$$

For specified β and given $\bar{J}_\ell$ there is an associated cross-sectional area ΔS_ℓ which in general is also a function of the particle diameter d. However, for the case where ΔS_ℓ is independent of d, a simpler form for $\underline{\underline{\Delta S}}$ results.

In the equation set (4.12), the contribution to C_i from N_j $(j > i)$ is $U\,\Delta S_{ij}\,N_j$. Such contributions can be assumed to be generated in the region of the measurement volume with value $\bar{J}_\ell$ having area ΔS_ℓ, so that

$$\bar{A}_i = \bar{J}_\ell\,\bar{F}_j \qquad \text{(II.3)}$$

But, in view of relations (II.1) and (II.2) we also have

$$\bar{A}_{i+1} = \bar{J}_\ell\,\bar{F}_{j+1}$$

Hence, it follows that

$$\Delta S_{ij} = \Delta S_{i+1,\ j+1} = \Delta S_{\ell} \qquad \text{(II.5)}$$

i.e., all the elements along any given diagonal in the ΔS_{ij} matrix are equal. Furthermore, since it is clear that ℓ is constant if (j-i) is constant, and in view of (II.3), then the relation between the indexing schemes is $\ell = m - (j-i)$, i.e.,

$$\Delta S_{ij} = \Delta S_{m-(j-i)} \qquad \text{(II.6)}$$

Thus we have shown that when $\bar{J}$ is not a function of d and intervals of $\Delta\bar{A}_i$, $\Delta\bar{F}_j$ and $\Delta\bar{J}_{\ell}$ are chosen to be logarithmic (Eqns II.1 and II.2), the general form of the ΔS matrix appearing in Eq (4.12) reduces to that of Eq (4.17).

Physically this means that for all pairs of (i,j) values such that (i-j) = (m-ℓ), signals in the amplitude class $\bar{A}_i$ arising from particles yielding response functions in the class $\bar{F}_j$ are generated in exactly the same part of the measurement volume ΔS_{ℓ} corresponding to the value $\bar{J} = \bar{J}_{\ell}$.

The question arises of what physical conditions have to be satisfied in order that $\bar{J}$ should be independent of d, and how can one check experimentally that the condition is fulfilled. Clearly, one necessary condition is that the largest particle to be measured (in the class d_m corresponding to the response function class $\bar{F}_m$) should be reasonably small compared to the dimensions of the measurement volume, in particular the radius w_o of the laser beam. Otherwise, such particles will not experience an incident wave that is approximately a uniform one, as is required by the Mie theory. Most likely there are other conditions related to the imaging of the particle onto the collection aperture which must be satisfied in order that $\bar{J}$ should be independent of d. However, these are difficult to specify, since they probably involve the quality of the collection lens with respect to abberations.

In view of such uncertainties in specifying the necessary and sufficient conditions that $\bar{J}$ should be independent of d, we have taken a pragmatic approach, and devised an experimental test which confirmed, at least for the experimental conditions employed, that $\bar{J}$ was indeed sensibly independent of d. This experimental test can be explained as follows. At the end of Sec. 4.2, an extension of the basic calibration technique was described that allows the

absolute concentration N_m and hence the absolute values of the ΔS_ℓ matrix, to be determined, using the largest size monodisperse particles of interest. The procedure involved summing the count rates C_i from channels $i = m$ down to $i = (m-r)$, i.e., over the top $(r+1)$ channels, and using the relation (see Eqn. 4.19)

$$C_{m-r,r} = U\, S_{m-r,m}\, N_m \tag{II.7}$$

The value of $S_{m-r,m}$, the cross-sectional area of the measurement volume over which $\bar{J}$ lies between $\bar{J}_m = 1$ and $\bar{J}_{m-r} = 1/(1+\beta)^r$ is found by traversing a small pinhole through the measurement volume. The test of the independence of $\bar{J}$ on d consists of repeating this procedure for different, small sizes of monodisperse particles (Table 5.1).

For particles of size class d_k, and concentration N_k, the sum of the count rates in the $(r+1)$ channels from $i = (k-r)$ to $i = k$ is given by

$$C_{k-r,k} = U\, S_{k-r,k}\, N_k \tag{II.8}$$

provided that $\bar{J}$ is not a function of d. Under the same condition, if r is held constant in the two measurements,

$$S_{k-r,r} = S_{m-r,r} \tag{II.9}$$

so that the same area, determined using the pinhole traversing technique, can be used in Eqn. 11.8 as in Eqn. 11.7. Hence the absolute value of N_k is determined in the same fashion as N_m.

Now the measurement of N_m allowed the absolute values of the ΔS_ℓ determined, for $\ell = 1$ to m from (Eqn. 4.16)

$$C_\ell = U\, \Delta S_\ell\, N_m\,. \tag{II.10}$$

Likewise, the measurement of N_k allows an independent set of absolute values of the ΔS_ℓ to be determined for $\ell = (m-k)$ to m from the equation set

$$C_i = U\, \Delta S_\ell\, N_k \tag{II.11}$$

where $\ell = m-(k-i)$, and i ranges from 1 to k. It follows from Eqns. II.8 and II.10 that

$$\frac{\Delta S_{m-(k-i)}}{S_{k-r,k}} = \frac{C_i}{C_{k-r,k}} \quad , \quad i = 1,k \, . \qquad \text{(II.13)}$$

Thus values of $\Delta S_{m-(k-i)}$ normalized on a fixed reference area $S_{k-r,r}$ can be determined without knowledge of the number concentration N_k. This equation is valid even if $\bar{J}$ has a particle size dependence, as long as the reference area $S_{k-r,r}$ is determined for each particle size d_k. For the case where $\bar{J}$ is independent of d_k, then $S_{k-r,k} = S_r$ for all N_k.

APPENDIX III ERROR ANALYSIS OF INVERSION TECHNIQUE

There are two sources of errors in computing values of particle number density, N_m, namely random counting errors in C_i and errors in specifying correct values for the elements of $\underline{\underline{\Delta S}}$. Counting errors, which derive from a finite sampling time, can be readily evaluated according to Poisson statistics. We have assumed that all particles and particle size classes have an equal probability or passing through any point of the measurement cross-section. This assumption is true only as C_i approaches infinity. For a 95% confidence level Poisson statistics give

$$\left|\frac{\Delta C_i}{C_i}\right| \simeq \frac{2}{\sqrt{C_i}} \qquad \text{(III.1)}$$

where ΔC_i = random error in C_i

C_i = measured number count

According to the above relation one should acquire a minimum of 1000 counts in each size range channel to achieve a ±6% error in C_i.

The effects of these counting errors on the uncertainty in N_i cannot be quantified without making some approximations for the form of $\underline{\underline{\Delta S}}$. For a Gaussian illumination beam it turns out that the individual cross-section elements are all nearly equal. The following analysis assumes that they <u>are</u> identical and known. For $\Delta S_{ij} = \Delta S$ for all i, j the equation set 4.17 becomes

$$\begin{aligned} C_1 &= (N_1+N_2+ \ldots + N_m)\ U\ \Delta S \\ C_2 &= \quad N_2+ \ldots + N_m)\ U\ \Delta S \\ &\cdots \\ C_m &= \quad (N_m)\ U\ \Delta S \end{aligned} \qquad \text{(III.2)}$$

To simplify the problem we choose a velocity U such that $U\ \Delta S = 1$. If there were no uncertainties in the individual ΔS_{ij} then we would obtain

$$N_i = C_i - C_{i+1}, \quad i = 1, m-1 \qquad \text{(III.3)}$$

The uncertainty in N_i would be given by

$$\left|\frac{\Delta N_i}{N_i}\right| = \sqrt{\left(\frac{\Delta C_i}{C_i}\right)^2 + \left(\frac{\Delta C_{i+1}}{C_{i+1}}\right)^2} \qquad \text{(III.4)}$$

or

$$\left|\frac{\Delta N_i}{N_i}\right| = 2\sqrt{\frac{1}{C_i} + \frac{1}{C_{i+1}}}$$

If $C_i \leq 1000$ then $\left|\Delta N_i\right| / N_i \leq 0.09$ from random counting errors.

The potential errors in the computed number distribution $\underline{N}$ due to uncertainty in the elements of $\underline{\underline{\Delta S}}$ require numerical calculations using perturbed valu of $\underline{\underline{\Delta S}}$. As shown in Figure 12 an average curve with a deviation of ±10% characterizes $\Delta S_{m-(k-i)}$. Although values of the <u>true</u> $\underline{\underline{\Delta S}}$ elements would be expected to vary systematically with increasing particle size, we will assume that the measurement errors are random within the range of the five sets of experimental results. This approach will provide an upper bound for the error estimate.

For numerical analysis of the effect of uncertainties in $\underline{\underline{\Delta S}}$, artifically perturbed values of $\underline{\underline{\Delta S}}$ were generated by using the following equation,

$$\Delta S_{ij} = \overline{\Delta S}_{ij} \ (0.9 + 2\varepsilon RN) \qquad \text{(III.5)}$$

where $\overline{\Delta S}_{ij}$ is a mean experimental value, ε is the maximum fractional deviation from $\overline{\Delta S}_{ij}$, and RN is a random number between zero and one. Three sets of $\underline{\underline{\Delta S}}$ were generated, and using a given count distribution $\underline{C}$, three number distribution solutions $\underline{N}$, shown in Table III.1 were obtained. The overall standard deviation between the average of $\underline{N}$ for the three perturbed solutions and the $\underline{N}$ for $\Delta S_{ij} = \overline{\Delta S}_{ij}$ is ±5 cm^{-3}. Although greater deviations from the average occur for the perturbed solutions (e.g. channel 13), it should be noted that these large deviations are compensated by a corresponding deviation of the opposite sign in an adjacent channel. In other words, size resolution and number resolution are coupled. Forcing better size resolution produces greater errors in the number density for each size range and vice versa. The upper bound for combined uncertainty from random counting errors (c.e.) and uncertainty in $\underline{\underline{\Delta S}}$ is given by

Table III.1. Comparison of N_1 for Perturbed and Average Values of $\underline{\underline{\Delta S}}$.

CHANNEL NUMBER	N_1 (cm^{-3})				
	Perturbed $\underline{\underline{\Delta S}}$ Solutions			Average of Perturbed Solutions	Solution For Average ΔS
	1	2	3		
1	0	0	0	0	0
2	0	0	0	0	0
3	0	0	0	0	0
4	0	0	0	0	0
5	0	0	0	0	0
6	0	0	0	0	0
7	0	0	0	0	0
8	0	0	0	0	9
9	89	88	91	90	92
10	7.5	14.7	0	7.4	0
11	0	0	7.8	2.6	7.8
12	8.2	0	0	2.7	0
13	3.5	19	24	6.3	9.7
14	64	50	41	52	56
15	0	0	0	0	0
16	0	2.7	13.4	5.4	0
17	38	38	39	38	46.8
18	8.0	11	0	6.4	10.4
19	11	4.1	9.6	8.2	0
20	26	30	30	28.4	31

$$\frac{\Delta N_i}{N_i} = \pm\sqrt{\left(\frac{\Delta N_i}{N_i}\right)^2_{CE} + \left(\frac{\Delta N_i}{N_i}\right)^2_{\Delta S}} \qquad \text{(III.6)}$$

For the results of Figure 14, the greatest uncertainty occurs in channel 20 and is

$$\left.\frac{\Delta N_i}{N_i}\right|_{20} = \pm\sqrt{(.2)^2 + \left(\frac{5}{31}\right)^2}$$

$$= \pm 26\%.$$

For larger number density flows (as occur in practice) or for longer sampling times, counting errors can be significantly reduced. Reduced counting errors will also reduce the uncertainty in $\underline{\underline{\Delta S}}$.

REFERENCES

[1] Cadle, R. D., The Measurement of Airborne Particles, Wiley & Sons, New York, 1975.

[2] Allen, T. Particle Size Measurement, Halsted Press, 1975.

[3] Van De Hulst, H. C., Light Scattering by Small Particles, John Wiley & Sons, 1957.

[4] Kerker, M., The Scattering of Light and Other Electromagnetic Radiation, Academic Press, 1969.

[5] McCreath, C., Roett, M., Chigier, N., "A Technique for Measurement of Velocities and Size of Particles in Flames," J. Phys. E., 5, 601 (1972).

[6] Belz, R., Dougherty, N., "In-Line Holography of Reacting Liquid Sprays," Proc. Engin. Applications of Holography, Feb. 1972, Los Angeles, Calif.

[7] Hodkinson, J., "The Optical Measurement of Aerosols," Ch X of Aerosol Science, ed C. Davies, Academic Press, 1966.

[8] Holve, D., Self, S., "Optical Measurements of Mean Particle Size in the Exhaust of a Coal-Fired MHD Generator," Fall, 1976 meeting of Western States Section of the Combustion Institute, La Jolla, Calif.

[9] Dobbins, R., Crocco, L., Glassman, I. "Measurement of Mean Particle Sizes of Sprays from Diffractivly Scattered Light," AIAA Journal, Vol 1, #8, Aug. 1963, pp. 1882-1186.

[10] Wertheimor, A., Wilcock, W., "Light Scattering Measurements of Particle Distributions," Appl. Optics, Vol. 15, No. 6, June 1976.

[11] Swithenbank, J., Beer, J., Taylor, D., "A Laser Diagnostic Technique for the Measurement of Droplet and Particle Size Distribution," AIAA 14th Aerospace Science Meeting, Wash., D.C., Jan. 1976.

[]2] Liu, Berglund, Agarwal, "Experimental Studies of Optical Particle Counters, Atmos. Envir., 8, 717, 1974.

[13] Cooke & Kerker, "Response Calculations for Light-Scattering Aerosol Particle Counters," Appl. Opt., 14, 734 (1975).

[14] Farmer, W. M., "Measurement of Particle Size, Number Density, and Velocity Using a Laser Interferometer," Appl. Opt. 11, 2603, 1972.

[15] Farmer, W. M., "Observation of Large Particles with a Laser Interferometer, Appl. Opt. 13, 610, 1974.

[16] Durst, I., "Development and Application of Optical Anemometer," Ph.D. Thesis, Univ. of London, 1972.

[17] Adrian, R., Orloff, K., "Laser Anemometer Signals: Visibility Characteristics and Application to Particle Sizing," Appl. Optics, Vol. 16, #3, March 1977.

[18] Adrian, R., Early, W., "Proc. of the Minnesota Symp. on Laser Anemometry," U. Minn., Dept. of Conferences, Minneapolis, 1976, p. 426.

[19] Hirleman, E., Wittig, S., "In Situ Optical Measurement of Automobile Exhaust Gas Particulate Size Distributions: Regular Fuel and Methanol Mixtures," 16th Symposium (International) on Combustion, MIT, August 1976.

[20] Hodkinson, J., Greenleaves, I., "Computations of Light-Scattering and Extinction by Spheres According to Diffraction and Geometrical Optics, and Some Comparisons with Mie Theory," J. of Opt. Soc. of Am., Vol. 53, #5, May 1963.

[21] Lieberman, A., Allen, R., "Theoretical and Experimental Light-Scattering Data for a Near Forward System," presented at American Association for Contamination Control, May 19-22, 1969.

[22] Oeseburg, F., "The influence of the Aperture of the Optical System of Aerosol Particle Counters on the Response Curve," J. of Aersol Science, Vol. 3, p. 307, 1972.

[23] Dave, J. V., "Subroutines for Computing the Parameters of the Electromagnetic Radiation Scattered by a Sphere," IBM Palo Alto Scientific Center Report No. 320-3237, May 1968.

[24] Ariessohn, P., Private Communication.

[25] Brooks, R., Chiro, G., "Principles of Computer-Assisted Tomography (CAT) in Radiographic and Radioisotopic Imaging," Physics of Medical Biology, Vol. 21, #5, 1976.

[26] Lawson, C., Hanson, R., Solving Least Squares Problems, Prentice Hall, Inc., N.J., 1974.

[27] Berglund, R., Liu, B., "Generation of Monodisperse Aerosol Standards," Envir. Sci. Technology, I, 1973, p. 147.

[28] Cadle, R., "The Measurement of Airborne Particles," J. Wiley, 1975, p. 75.

[29] Marple, V., Rubow, K., "Aerodynamic Particle Size Calibration of Optical Particle Counters," J. Aerosol Sci., Vol. 7, p. 425, 1976.

[30] Marple, V., Rubow, K., "A Portable Optical Particle Counter System for Measuring Dust Aerosols," paper submitted to American Industrial Hygiene Association Journal, December 1976.

SECURITY CLASSIFICATION OF THIS PAGE (When Data Entered)

REPORT DOCUMENTATION PAGE

READ INSTRUCTIONS BEFORE COMPLETING FORM

1. REPORT NUMBER: SQUID-SU-2-PU	2. GOVT ACCESSION NO.
3. RECIPIENT'S CATALOG NUMBER	
4. TITLE (and Subtitle): AN OPTICAL PARTICLE-SIZING COUNTER FOR IN-SITU MEASUREMENTS.	5. TYPE OF REPORT & PERIOD COVERED: Technical rept.
6. PERFORMING ORG. REPORT NUMBER	
7. AUTHOR(s): Don Holve and Sidney A. Self	8. CONTRACT OR GRANT NUMBER(s): N00014-75-C-1143
9. PERFORMING ORGANIZATION NAME AND ADDRESS: Mechanical Engineering Department, Stanford University, Stanford, California 94305	10. PROGRAM ELEMENT, PROJECT, TASK AREA & WORK UNIT NUMBERS: NR-098-038
11. CONTROLLING OFFICE NAME AND ADDRESS: Project SQUID, Chaffee Hall, Purdue University, West Lafayette, Indiana 47907	12. REPORT DATE: Jan 78; NUMBER OF PAGES: 68 (70 pp.)
14. MONITORING AGENCY NAME & ADDRESS (if different from Controlling Office): Office of Naval Research, Power Program, Code 473, Department of the Navy, 800 No. Quincy St., Arlington, VA 22217	15. SECURITY CLASS. (of this report): Unclassified
	15a. DECLASSIFICATION/DOWNGRADING SCHEDULE

16. DISTRIBUTION STATEMENT (of this Report)

This document has been approved for public release and sale; its distribution is unlimited.

17. DISTRIBUTION STATEMENT (of the abstract entered in Block 20, if different from Report)

Same

18. SUPPLEMENTARY NOTES

19. KEY WORDS (Continue on reverse side if necessary and identify by block number)

Optical Particle Sizing
Mie Scattering

20. ABSTRACT (Continue on reverse side if necessary and identify by block number)

A particle sizing counter is described, suitable for in-situ measurements in two phase flows of laboratory scale. It employs near-forward scatter from the focus of a He-Ne laser beam, together with pulse height-analysis of the signals from individual particles. A novel and essential feature of the technique is a numerical inversion scheme to unfold the dependence of the scattered signals on particle trajectory through the measurement volume. The inversion procedure is performed by an on-line computer, and utilizes a prior calibration with monodisperse aerosols of known size. As presently configured,

DD FORM 1 JAN 73 1473 EDITION OF 1 NOV 65 IS OBSOLETE
S/N 0102-014-6601 |

Unclassified
SECURITY CLASSIFICATION OF THIS PAGE (When Data Entered)

403 617

the instrument has a demonstrated capability of determining size distributions in the diameter range 2-25 μm, at concentrations up to ~10^5 cm^{-3}. The measured dependence of response on particle diameter agrees well with calculations from Mie scattering theory. It is anticipated that the technique can be extended to cover particle diameters up to at least 50 μm, and down to 0.5 μm and concentrations up to 10^6 cm^{-3}. It should also be adaptable to hot flows and absorbing, irregular particles.